

Lithium elemental and isotopic disequilibrium in minerals from peridotite xenoliths from Shangzhi, NE China: products of recent melt/fluid-peridotite interaction

Shenghua Zhou^{1,2} · Songyue Yu¹ · Ting Zhou¹ · Jiangbo Lan¹ · Jian Kang^{1,2} ·
Liemeng Chen¹ · Junhao Hu^{1,2}

Received: 19 December 2017 / Revised: 18 March 2018 / Accepted: 8 May 2018 / Published online: 18 May 2018
© Science Press, Institute of Geochemistry, CAS and Springer-Verlag GmbH Germany, part of Springer Nature 2018

Abstract Lithium elemental and isotopic disequilibrium has frequently been observed in the continental and oceanic mantle xenoliths, but its origin remains controversial. Here, we present a combined elemental and Li isotopic study on variably metasomatised peridotite xenoliths entrained in the Cenozoic basalts from Shangzhi in Northeast (NE) China that provides insight into this issue. Li concentration (0.3–2.7 ppm) and $\delta^7\text{Li}$ (mostly 2‰–6‰) in olivine from the Shangzhi peridotites are similar to the normal mantle values and show roughly negative correlations with the indices of melt extraction (such as modal olivine and whole rock MgO). These features are consistent with variable degrees of partial melting. In contrast, clinopyroxene from the Shangzhi xenoliths shows significant Li enrichment (0.9–6.1 ppm) and anomalously light $\delta^7\text{Li}$ (−13.8‰ to 7.7‰) relative to normal mantle values. Such features can be explained by Li diffusion from silicate melts or Li-rich fluids occurring over a very short time (several minutes to several hours). Moreover, the light Li isotopic compositions preserved in some bulk samples also indicate that these percolated melts/fluids have not had enough time to isotopically equilibrate with the bulk peridotite. We thus emphasize that Li isotopic fractionation in the Shangzhi mantle xenoliths is mainly related to Li diffusion from silicate melts or Li-rich fluids that took place shortly before or coincident with their entrainment into the host magmas.

Keywords Mantle peridotite · Li isotope · Mantle metasomatism · Northeastern China

1 Introduction

Lithium (Li) and its isotopes (${}^6\text{Li}$ and ${}^7\text{Li}$) were regarded as a very useful tools for tracking fluid-related processes and the recycling of surface materials to the mantle due to their moderate incompatibility, strong fluid mobility, large mass difference (~17%), and significant isotopic fractionation at low temperatures near the surface (e.g., Tomascak et al. 2002, 2016; Tomascak 2004; Elliott et al. 2004, 2006; Tang et al. 2007a, 2014).

To date, studies of Li isotopes in mantle xenoliths reveal a great range of $\delta^7\text{Li}$ in coexisting minerals (40‰) (Tang et al. 2010; Su et al. 2016; Penniston-Dorland et al. 2017) that contrasts with the relatively uniform $\delta^7\text{Li}$ of MORBs (+2‰ to +6‰), which samples the convecting mantle (Chan et al. 1992; Tomascak et al. 2008). The origin of such striking isotopic fractionation still remains elusive. Theoretical and case studies have proved that equilibrium fractionation of Li isotopes during high temperature processes, such as mantle partial melting and magma fractionation, is negligible (<1.0‰) (e.g., Tomascak et al. 1999; Chan and Frey 2003) while Su et al. (2017a) and Xiao et al. (2017) argued that Li isotopic fractionation during magma differentiation and partial melting are more significant. In addition, the diffusion process typically produces striking isotopic fractionation due to the exceptionally high diffusivity of Li and faster diffusion of ${}^6\text{Li}$ than ${}^7\text{Li}$ (Richter et al. 2003; Coogan et al. 2005). The Li diffusion process in mantle xenoliths may happen during slow cooling of mantle xenoliths after the eruption of their host magmas (Ionov and Seitz 2008; Gao and Snow 2011).

✉ Songyue Yu
yusongyueyig@hotmail.com

¹ State Key Laboratory of Ore Deposit Geochemistry, Institute of Geochemistry, Chinese Academy of Sciences, Guiyang 550081, PR China

² University of Chinese Academy of Sciences, Beijing 100049, PR China

This process may also relate to the interaction of peridotites with percolating melts (and/or host magmas) with normal mantle-like $\delta^7\text{Li}$ shortly before or coincident with their entrainment into the host magmas (Jeffcoate et al. 2007; Rudnick and Ionov 2007; Magna et al. 2008; Su et al. 2014b) or with recycled melt with low $\delta^7\text{Li}$ (Nishio et al. 2004; Tang et al. 2007b, 2012, 2014; Ackerman et al. 2013; Su et al. 2016). Metasomatism, by hypothetical isotopically light components derived from subducted oceanic slab, was proposed to explain high Li concentrations and low $\delta^7\text{Li}$ found in bulk and individual minerals from mantle xenoliths in eastern Asia (e.g., Nishio et al. 2004; Tang et al. 2007b, 2011, 2012; Zhang et al. 2010; Su et al. 2012). In contrast, Magna et al. (2008) argued that metasomatism by “subduction-related” components was not likely to strongly affect Li isotopic compositions in the lithospheric mantle. Previous studies also found strong inter-mineral Li-isotope disequilibria in most xenoliths suites. Some researchers proposed that Li-isotope disequilibria are related to the different behaviors of Li in silicate and in carbonatite metasomatism (Seitz and Woodland 2000; Su et al. 2012, 2014a, 2017b). Other researchers emphasized that the disequilibria is not likely to be preserved in the mantle for a long time and is therefore attributed to diffusion-controlled interaction with Li-bearing melt/fluid shortly before or during the transport of the xenolith to the surface (Jeffcoate et al. 2007; Rudnick and Ionov 2007; Aulbach et al. 2008; Aulbach and Rudnick 2009; Xu et al. 2013a, b). More recently, Xiao et al. (2017) suggested that the Li isotopic heterogeneity in the mantle is related to variable degrees of partial melting.

Here, we reported Li concentrations and isotopic compositions of pure olivine and clinopyroxene (Cpx) separates from variably metasomatised peridotite xenoliths from Shangzhi, NE China. The Shangzhi samples show negative $\delta^7\text{Li}$ values and abnormally high Li concentrations in Cpx and strong Li disequilibria between coexisting olivine and Cpx. We emphasize that Li isotopic fractionation in the Shangzhi mantle xenoliths is mainly related to Li diffusion from silicate melts or Li-rich fluids occurring shortly before or coincident with their entrainment into the host magmas.

2 Geological background and sample description

Northeast China (NE China) is located in the eastern part of the Central Asian Orogenic Belt (CAOB), which was considered as a composite fold belt formed by amalgamation of several minor blocks (e.g., Xing'an, Songliao, Jamusi, etc.) during subduction and collision between the North China Craton (NCC) and the Siberian Craton (Xu et al. 2013a, 2013b; Liu et al. 2016). Since the Late

Mesozoic, NE China became an important part of the circum Pacific tectonic–magmatic belt. During the Cenozoic time, intraplate basaltic magmatism was widely distributed in the Songliao Basin and its surrounding areas (Fig. 1a). In an area of about two million square kilometers, there are over 590 volcanoes with basaltic rocks covering about 50,000 km² (Fig. 1a; Liu 1999; Ma et al. 2002). The basaltic rocks have been grouped into three successive episodes: (1) Late Cretaceous–Paleogene sub-alkaline and alkaline basalts; (2) Neogene alkali basalts with a minor amount of tholeiitic basalts, and (3) Quaternary alkaline basalts (Fan and Hooper 1989; Liu et al. 1992). Mantle xenoliths, mainly spinel lherzolite and harzburgite, are mostly found in the Neogene and Quaternary alkaline basalts and are generally not found in the tholeiitic flows. Numerous studies have been conducted on these rocks (e.g., Basu et al. 1991; Tatsumoto et al. 1992; Zhang et al. 2000; Xu et al. 1998, 2003; Yu et al. 2009, 2010).

The peridotite xenoliths in this study were collected from the Shangzhi volcanic field in Heilongjiang Province (Fig. 1). The Shangzhi volcanic field is located along northern edge of the Songliao basin and occurs within the Yilan-Shulan fault zone (Fig. 1a). The volcanic rocks in Shangzhi are Neogene alkali basalts (~ 13 Ma) varying from nepheline to olivine basanite (Liu et al. 1992). Abundant fresh spinel peridotite xenoliths entrained by alkali basalts, 5–25 cm in diameter, were discovered in a quarry at Guixiang village. Thirteen spinel lherzolites and eight spinel harzburgites were collected from this locality and used in this study.

All studied xenoliths are fresh anhydrous peridotites and belong to the Group I peridotites of Frey and Prinz (1978). They are spinel peridotites ranging from lherzolites (Cpx > 5%) to harzburgites (Cpx < 5%). Mineral assemblage for harzburgites is olivine (Ol, 70%–86%), orthopyroxene (Opx, 10%–25%), clinopyroxene (Cpx, 2%–4%) and spinel (Sp, 1%–3%) (Table 1). Among the harzburgites, samples with protogranular texture are the most abundant (Fig. 2a). Mineral grains in these samples are characterized by a coarse grain size of 3–5 mm. Olivine and Opx grains are equant and exhibit curvilinear grain boundaries. Large olivine grains (> 4 mm) are kinked. Some of them contain small inclusion of spinel (0.1–0.2 mm). The typical mineral assemblage for lherzolites is olivine (54%–75%), Cpx (6%–18%), Opx (14%–29%) and spinel (1%–5%) (Table 1). Lherzolites from this region are characterized by equigranular texture with medium grain size (1–1.5 mm in diameter) and occasional porphyroblasts of Opx (Fig. 2b). They are partially recrystallized and show a nearly 120 °C triple junction (Fig. 2b). Most Cpx in lherzolites are generally green and clear, but some (e.g., GX-14) display a spongy appearance (Fig. 2c). Most spinel grains are anhedral and occur as an

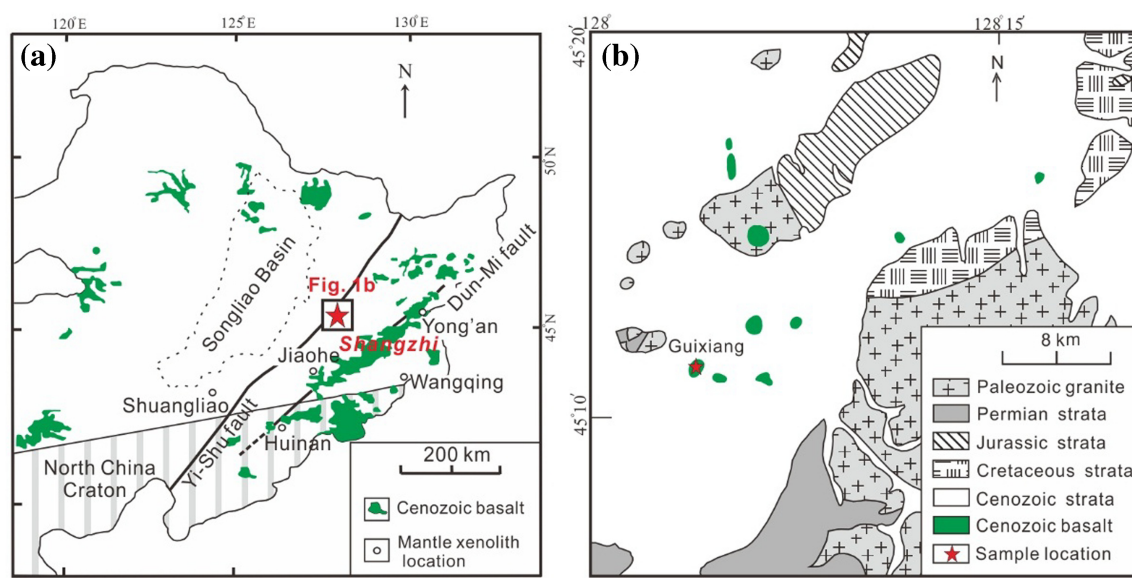


Fig. 1 **a** Simplified tectonic scheme and distribution of Cenozoic basalts in northeastern China and location of the studied area. Samples used in this study were collected from Guixiang, Shangzhi City. Yi-Shu fault and Dun-Mi fault represent Yilan–Shulan fault zone and Dunhua–Mishan fault zone respectively; **b** enlarged sampling area in Shangzhi, Northeastern China

Table 1 Modal composition of Shangzhi peridotite xenoliths (vol%)

Sample	Rock type	Texture	Modal composition			
			Ol	Opx	Cpx	Sp
GX-2	Lherzolite	Equigranular	57	22	18	3
GX-3	Lherzolite	Equigranular	75	16	8	1
GX-4	Lherzolite	Equigranular	57	24	15	4
GX-5	Lherzolite	Equigranular	58	23	15	4
GX-7	Lherzolite	Equigranular	54	23	18	5
GX-8	Lherzolite	Equigranular	75	14	9	2
GX-9	Lherzolite	Equigranular	66	24	8	2
GX-11	Lherzolite	Equigranular	65	22	11	2
GX-12	Lherzolite	Equigranular	65	24	10	1
GX-14	Lherzolite	Equigranular	59	24	15	2
GX-15	Lherzolite	Equigranular	57	29	12	2
GX-16	Lherzolite	Equigranular	70	22	6	2
GX-19	Lherzolite	Equigranular	63	25	10	2
GX-1	Harzburgite	Protogranular	75	18	4	3
GX-6	Harzburgite	Protogranular	84	12	2	2
GX-10	Harzburgite	Protogranular	74	20	4	2
GX-13	Harzburgite	Protogranular	82	15	2	1
GX-17	Harzburgite	Protogranular	84	13	2	1
GX-18	Harzburgite	Protogranular	86	10	3	1
GX-20	Harzburgite	Protogranular	70	25	4	1
GX-21	Harzburgite	Protogranular	76	20	3	1

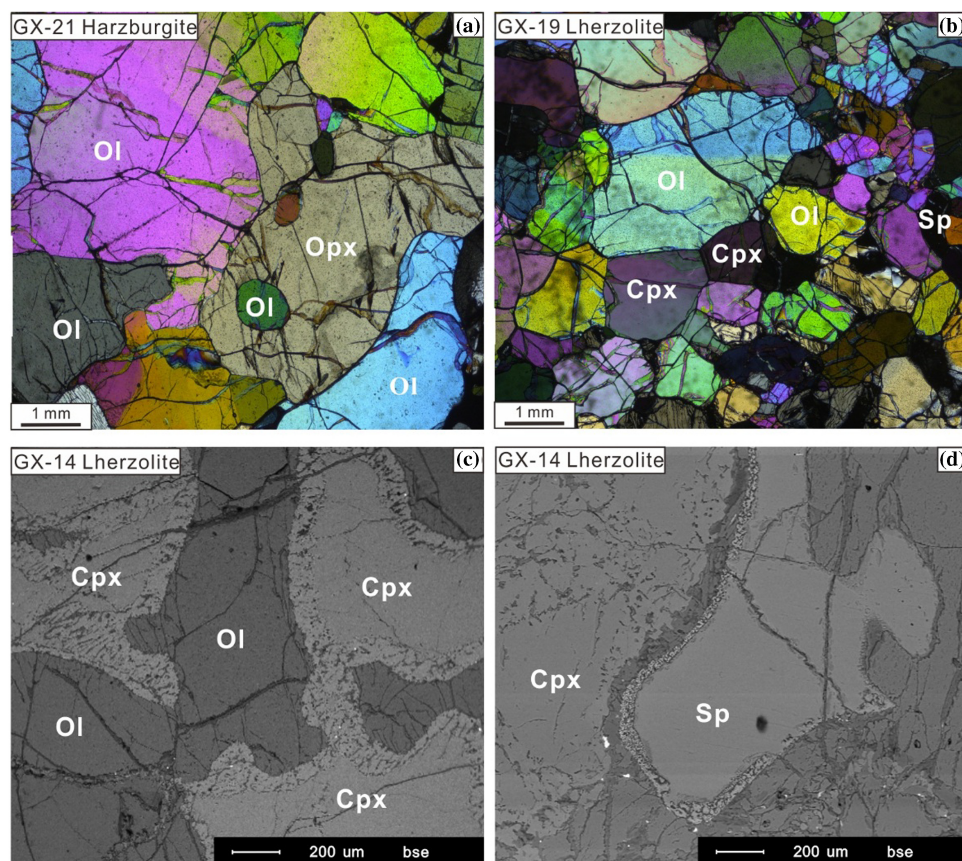
Ol olivine, Cpx clinopyroxene, Opx orthopyroxene, Sp spinel, modal composition were calculated by a least-square fit method using constituent mineral chemistry and bulk geochemistry

interstitial phase among silicate minerals. Some of them also display a spongy texture (Fig. 2d).

3 Analytical methods

The xenoliths in this study were cut to remove exterior surfaces. Relatively fresh interiors without basaltic veins were used for bulk-rock analyses and for mineral separation. The rocks were crushed and sieved with stainless sieves. Olivine and Cpx were handpicked under a binocular microscope. Only the most pure and fresh mineral grains were selected for Li isotope analysis. These separates were then washed in an ultrasonic bath three times with Mill-Q ultra-pure water. The mineral separates and whole rock samples were then ground to 200 mesh powders using an agate mortar. The major elements were analyzed using a PANalytical Axios-advance X-ray fluorescence spectrometer (XRF) on fused glass beads in the laboratory of ALS Chemex Ltd in Guangzhou, China. The analytical errors were mostly < 5%. Loss on ignition (LOI) was determined by heating a 1 g power sample to 1100 °C for 1 h. The major element compositions of minerals were analyzed using the EMPA-1600 electron microprobe at the Institute of Geochemistry, Chinese Academy of Sciences (IGCAS). Analytical conditions for major elements were 25 kV accelerating voltage, 10 nA beam current and 10 μm beam size. The detection limit for major elements under such conditions is 0.01 wt%. The analytical reproducibility was within 2% for major elements. The trace element compositions of Cpx separates were analyzed using an

Fig. 2 **a** Photomicrographs of representative textures of the Shangzhi peridotite xenoliths. Protoplanular texture (crossed polarizer); **b** equigranular texture (crossed polarizer); **c–d** back-scattered secondary electron images displaying sieve-textured Cpx and spinel from the Shangzhi lherzolites; *Ol* olivine, *Opx* orthopyroxene, *Cpx* clinopyroxene, *Sp* spinel



Inductively Coupled Plasma-Mass Spectrometer (ICP-MS) at the Institute of Geochemistry, Chinese Academy of Science (IGCAS), following the analytical procedures described by Qi et al. (2000). The powdered samples (50 mg) were dissolved in a Hf + HNO₃ solution in high-pressure Teflon bombs that were heated at ~ 190 °C for 12 h. Rh was used as an internal standard to monitor signal shift during analysis. The USGS standard BHVO-2 and BCR-2 were determined as unknowns. The overall analytical precision is better than 5% relative to the recommended values (Table 4).

Separation of Li for isotopic composition analysis was undertaken in a clean lab at the University of Science and Technology of China (USTC) following the procedure described by (Gao and Casey 2012; Sun et al. 2016). Samples were initially dissolved in a 1:1 HNO₃-HF mixture solution, evaporated to dryness and treated two times with 8 N HCl. Finally the samples were dissolved in 3 mL 0.2 N HCl and loaded on cation exchange columns. Prior to Li isotope analysis, Na/Li ratios of all separations were measured semi-quantitatively using ICP-MS at USTC to guarantee both high Li yield (> 99.8% recovery) and low Na/Li ratio (< 0.5). The final concentration of Li in the solutions utilized for MC-ICP-MS analyses was targeted to

be about 50–200 ppb to ensure the best precision and accuracy.

Li isotopic compositions were analyzed at IGCAS using a Neptune Plus MC-ICP-MS (Thermo Fisher Scientific) and a standard-sample bracketing method. IRMM016 was utilized as the isotopic standard during analysis. All samples and reference solutions were introduced using a micro-flow nebulizer attached to a double-Scott spray chamber and ran in a block of 30 cycles of measurement with an integration time of 2 s. Typical sensitivity achieved was 50–60 V/ppm for ⁷Li at a flow rate of ~ 50 µL·min⁻¹. In-house standard L-SVEC and QC were measured every 3 samples to monitor the quality of measurement. The Li isotope ratios were calculated relative to the average of two bracketing IRMM-016 runs and reported as $\delta^7\text{Li}$ (‰) = [${}^{7}\text{Li} / {}^{6}\text{Li}$]_{sample}/ ${}^{7}\text{Li} / {}^{6}\text{Li}$]_{standard} - 1] × 1000. The external precision is less than 0.3‰ (2SD) based on long-term analysis of rock solutions and Li standard solutions over 2-years. The obtained $\delta^7\text{Li}$ values for international standards BHVO-2 and GSP-2 were $4.04\text{‰} \pm 0.04\text{‰}$ and $-0.89\text{‰} \pm 0.04\text{‰}$ (2SD) respectively, which were consistent with the previously published results (e.g., Simons et al. 2010; Vlastélic et al. 2011; Krienitz et al. 2012; Lin et al. 2016). The Li concentration in rock samples was measured by voltage comparisons with those obtained for

the L-SVEC reference material (of known concentration) and then adjusted for sample mass. The uncertainty in Li concentration determined by this method was less than $\pm 10\%$ (Teng et al. 2007).

4 Results

4.1 Whole-rock major element compositions

Whole-rock major element compositions of Shangzhi peridotites are listed in Table 2 and plotted in Fig. 3. The Shangzhi peridotites have very low (i.e., < 1%) loss on ignition (LOI) and display a considerable spread in major element composition, ranging from fertile lherzolites to refractory harzburgites with up to 46.6 wt% MgO. There are negative correlations between MgO and Al₂O₃ and CaO for Shangzhi peridotite xenoliths. Most samples lie

along the partial melting trends in Fig. 3a and are interpreted as residues of variable degrees of partial melting (Niu 1997). In contrast, most harzburgite samples and some lherzolite samples display significant enrichment of Na₂O compared with the partial melting trend (Fig. 3b).

4.2 Mineral chemistry

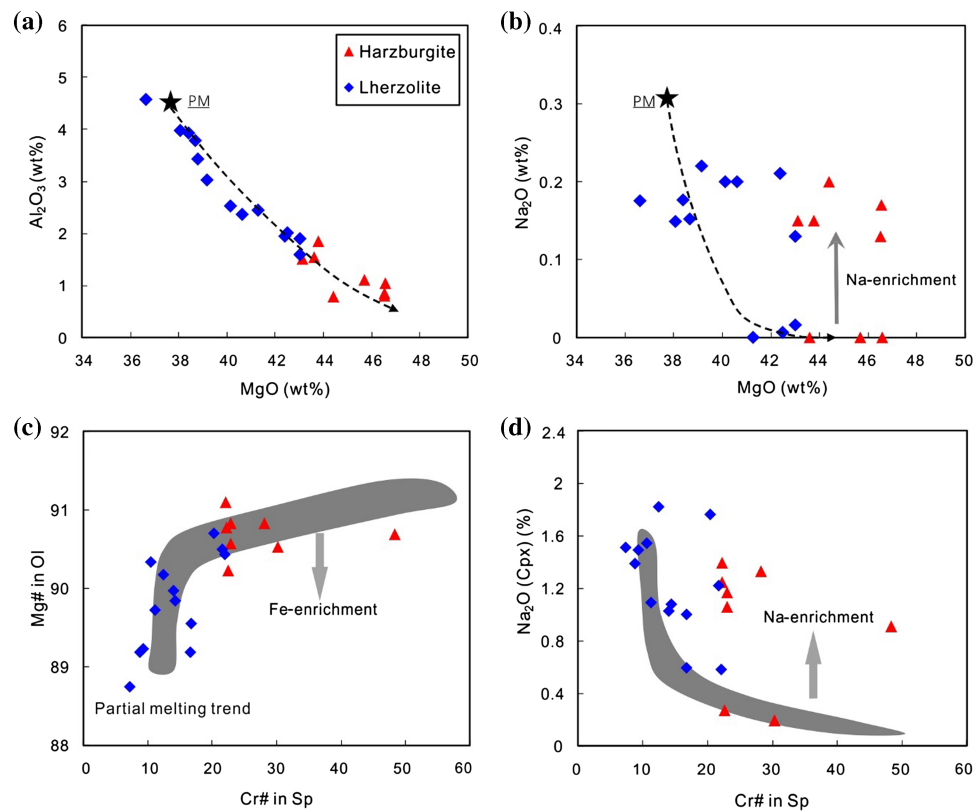
The minerals (olivine, Cpx and Opx) in Shangzhi peridotites are homogeneous in major oxides based on analyses by EPMA from core to rim. The average compositions are given in Table 3. The studied xenoliths display a wide range in mineral compositions, which matches the petrographic variation. Mg#_{ol} [100 × Mg/(Mg + Fe)_{at}] and Cr#_{sp} [100 × Cr/(Cr + Al)_{at}] in Shangzhi peridotites range from 88.8 to 91.1 and from 7.3 to 48.3, respectively. In the co-variation diagram of Mg#_{ol} versus Cr#_{sp} (Fig. 3c), most samples lie along the partial melting trend.

Table 2 Whole rock major element compositions of Shangzhi peridotite xenoliths

Sample	GX-2	GX-3	GX-4	GX-5	GX-7	GX-8	GX-9	GX-11	GX-12	GX-14	GX-15	GX-16	GX-19
Rock type	Lherzolite												
MgO	38.39	43.02	38.06	38.66	36.62	42.48	41.27	40.12	42.39	38.79	39.15	43.01	40.60
SiO ₂	44.79	43.92	44.31	44.12	44.49	43.26	44.68	44.39	44.34	44.3	45.11	43.75	44.39
Fe ₂ O ₃ _{Total}	8.08	8.18	8.64	8.85	8.50	9.39	8.62	8.50	8.41	8.29	8.59	8.60	8.57
TiO ₂	0.13	0.02	0.09	0.10	0.17	0.06	0.01	0.02	0.02	0.14	0.03	—	0.02
CaO	3.71	1.78	3.41	3.37	3.96	2.09	2.09	2.51	1.78	3.09	2.69	1.59	2.42
Al ₂ O ₃	3.93	1.91	3.98	3.78	4.59	2.02	2.46	2.54	1.95	3.43	3.03	1.60	2.37
MnO	0.11	0.10	0.12	0.12	0.12	0.12	0.11	0.13	0.12	0.12	0.13	0.12	0.13
Cr ₂ O ₃	0.32	0.22	0.25	0.23	0.23	0.20	0.26	0.43	0.39	0.41	0.44	0.40	0.39
Na ₂ O	0.18	0.02	0.15	0.15	0.17	0.01	—	0.20	0.21	0.41	0.22	0.13	0.20
P ₂ O ₅	0.01	0.01	0.01	0.02	0.01	0.01	0.01	0.03	0.02	0.04	0.01	0.01	0.03
Total	99.80	99.75	99.54	99.67	99.65	99.72	99.71	99.40	99.86	99.53	99.89	99.62	99.56
LOI	0.16	0.56	0.51	0.28	0.78	0.10	0.20	0.53	0.23	0.51	0.49	0.41	0.44
Sample	GX-1	GX-6	GX-10	GX-13	GX-17	GX-18	GX-20	GX-21					
Rock type	Harzburgite												
MgO	43.77	46.57	43.60	45.69	46.51	46.53	43.10	44.39					
SiO ₂	43.54	42.39	44.09	42.84	41.55	41.31	43.45	43.41					
Fe ₂ O ₃ _{Total}	8.69	8.94	8.64	8.33	9.06	9.04	8.50	8.52					
TiO ₂	—	—	—	0.03	0.01	—	—	—					
CaO	1.43	0.50	1.28	0.54	0.60	0.59	1.10	0.89					
Al ₂ O ₃	1.86	1.05	1.55	1.11	0.81	0.85	1.51	0.80					
MnO	0.12	0.11	0.11	0.11	0.12	0.12	0.12	0.13					
Cr ₂ O ₃	0.39	0.25	0.23	0.26	0.18	0.19	0.33	0.35					
Na ₂ O	—	—	—	0.13	0.17	0.15	0.20	0.15					
P ₂ O ₅	0.01	0.01	0.01	0.03	0.03	0.02	0.02	0.04					
Total	99.77	99.86	99.81	99.27	99.44	99.08	99.09	98.86					
LOI	— 0.03	0.02	0.29	0.20	0.40	0.28	0.76	0.18					

— Below detection limit

Fig. 3 **a–b** Plots of whole-rock MgO against Al₂O₃ and Na₂O; **c** correlation of Cr# (Cr/(Cr + Al_{atomic})) in spinel versus Mg# of olivine; **d** plot of Cr# in spinel versus Na₂O in Cpx; The black lines are near-fractional melting model trend of a starting source of primitive spinel peridotite using the model of Niu (1997). Primitive mantle compositions (PM) are after McDonough and Sun (1995). The partial melting trend is modeled using the fractional partial melting model of Johnson et al. (1990)



In contrast, Cpx in most samples shows fairly high Na₂O contents (0.2 wt%–1.8 wt%), which are significantly higher than expected from the partial melting trend (Fig. 3d). The Cpx grains with spongy texture shows compositional variations from the core to the spongy rim. The spongy rim is typically enriched in CaO, TiO₂ and depleted in Na₂O, Al₂O₃ compared with the core (Table 3). These observations are consistent with the interpretation that spongy-textured Cpx in peridotite xenoliths developed from a decompression-induced partial melting event (Su et al. 2011).

Cpx trace element compositions are listed in Table 4 and plotted in Fig. 4. Cpx in harzburgite shows enriched LREE [$(\text{La/Yb})_{\text{N}} = 0.75\text{--}39.79$], flat HREE [$(\text{Gd/Yb})_{\text{N}} = 0.65\text{--}2.37$] and variable enrichment of Th, U, Nb, Ta (Fig. 4a, b). Cpx in lherzolites shows both LREE-enriched [$(\text{La/Yb})_{\text{N}} = 0.93\text{--}3.75$] and LREE-depleted [$(\text{La/Yb})_{\text{N}} = 0.1\text{--}0.54$] patterns. In specific, Cpx in three lherzolite samples (GX-2, GX-3 and GX-4) displays both LREE-depleted patterns and weak positive anomalies of Th and U (Fig. 4d). Cpx in other lherzolite samples shows variable LREE enrichment and strong positive anomalies of Th and U (Fig. 4d). Two lherzolite samples (GX-12, GX-14) display strongest LREE enrichment and abnormally high contents of Nb and Ta in Cpx (Fig. 4c, d).

4.3 Li concentrations and isotopic compositions of mineral separates

Li contents and isotopic compositions in the Shangzhi peridotite xenoliths are listed in Table 5. Li concentrations in olivine range from 0.3 to 2.7 ppm, and these values are significantly lower than those in Cpx (0.9–6.1 ppm) (Table 5; Fig. 5a). This observation is consistent with previous studies of metasomatised peridotites in the North China Craton, where pyroxenes commonly show higher Li concentrations than olivine (Tang et al. 2007b, 2011, 2012, 2014; Zhang et al. 2010; Su et al. 2014a; Xiao et al. 2015). Almost all Shangzhi peridotites plot out of the range of “equilibrated” mantle peridotites (Fig. 5a; Seitz and Woodland 2000). Li contents of olivine are similar to the normal mantle, but those in Cpx are strikingly higher than the normal mantle (Fig. 5a; Ryan and Langmuir 1987; Jeffcoate et al. 2007; Magna et al. 2006; Seitz and Woodland 2000; Seitz et al. 2004). In the diagram of the partition coefficient for Li between olivine and Cpx ($\text{ol/cpx} D_{\text{Li}}$) versus the degree of isotopic equilibrium ($\Delta^7 \text{Li}_{\text{ol-cpx}}$; Fig. 5b), the Shangzhi peridotites display variable degrees of elemental and isotopic disequilibria. Such elemental and isotopic disequilibria were also observed in other metasomatically overprinted peridotite xenoliths (Seitz and Woodland 2000; Seitz et al. 2004; Rudnick and Ionov 2007; Jeffcoate et al. 2007; Su et al.

Table 3 Major element composition (wt%) of minerals from Shangzhi mantle xenoliths

Sample	GX-2			GX-3			GX-3									
	Lherzolite			Lherzolite			Lherzolite									
Rock	OI	Opx	Cpx	Sp	OI-c	OI-m	OI-r	Opx-c	Opx-m	Opx-r	Cpx-c	Cpx-m	Cpx-r	Sp		
Mineral																
Na ₂ O	—	0.10	1.54	—	—	—	—	0.12	0.12	0.10	1.38	1.33	1.31	—		
MgO	48.60	32.66	14.99	19.88	48.23	48.84	49.38	34.39	34.46	34.20	16.29	16.74	16.96	18.51		
Al ₂ O ₃	0.01	4.30	6.29	58.86	0.03	0.04	0.04	4.40	4.21	4.31	6.02	5.83	5.82	49.37		
SiO ₂	39.90	55.33	52.71	0.02	40.71	41.17	41.12	55.21	55.36	55.77	52.62	52.64	52.74	0.06		
CaO	0.04	0.67	20.00	—	0.07	0.05	0.08	0.72	0.60	0.64	20.04	19.57	19.91	—		
TiO ₂	—	0.12	0.54	0.16	—	0.03	0.04	0.10	0.04	0.08	0.26	0.21	0.26	0.11		
Cr ₂ O ₃	0.03	0.35	0.77	10.34	—	—	0.03	0.54	0.51	0.53	1.36	1.19	1.26	20.25		
MnO	0.10	0.14	0.09	0.09	0.08	0.12	0.12	0.15	0.10	0.11	0.07	0.09	0.06	0.14		
FeO	9.34	5.86	2.61	9.82	8.99	9.34	9.30	4.70	4.75	4.46	1.99	1.92	2.13	11.20		
NiO	0.32	0.07	0.04	0.35	0.39	0.36	0.37	0.13	0.11	0.08	0.04	0.09	0.09	0.27		
Total	98.35	99.58	99.58	99.51	98.51	99.94	100.47	100.48	100.25	100.27	100.07	99.62	100.55	99.91		
Mg#	90.3	90.9	91.2	78.4	90.6	90.4	90.5	92.9	92.9	93.2	93.6	94.0	93.5	74.8		
Cr#				10.5										21.6		
Sample	GX-4			GX-5			GX-7			GX-8						
Rock	Lherzolite			Lherzolite			Lherzolite			Lherzolite						
Mineral	OI	Opx	Cpx	Sp	OI	Opx	Cpx	Sp	OI	Opx	Cpx	Sp	OI	Opx		
Na ₂ O	—	0.03	1.49	—	0.01	0.02	1.39	—	—	0.01	1.51	0.01	—	0.06	1.00	
MgO	47.92	32.50	14.67	19.56	48.18	33.07	14.57	19.65	47.38	33.03	14.43	19.75	47.68	32.18	15.54	
Al ₂ O ₃	0.01	3.95	5.40	59.63	—	3.26	5.53	61.09	—	3.08	5.50	62.62	0.01	4.10	4.80	52.23
SiO ₂	40.31	54.92	52.95	0.04	40.34	56.10	51.97	0.02	40.86	55.89	53.97	0.02	40.59	54.71	52.55	0.02
CaO	0.01	0.51	21.41	—	0.03	0.36	21.05	0.01	0.01	0.28	21.81	—	0.04	0.80	21.28	—
TiO ₂	—	0.09	0.47	0.07	—	0.07	0.45	0.07	—	0.10	0.54	0.06	—	0.15	0.50	0.23
Cr ₂ O ₃	0.01	0.29	0.59	9.11	0.02	0.19	0.63	8.76	0.01	0.12	0.42	7.31	0.01	0.43	0.77	15.52
MnO	0.16	0.13	0.07	0.12	0.14	0.14	0.06	0.12	0.14	0.15	0.07	0.11	0.12	0.14	0.07	0.11
FeO	10.39	6.65	2.40	11.61	10.49	6.66	2.39	11.04	10.79	6.75	2.48	10.68	10.39	6.28	2.85	12.11
NiO	0.38	0.06	0.02	0.36	0.35	0.07	0.02	0.37	0.37	0.04	0.04	0.36	0.33	0.08	0.05	0.32
Total	99.19	99.13	99.47	100.50	99.55	99.94	98.96	101.12	99.56	99.44	100.78	100.93	99.17	98.92	99.40	99.17
Mg#	89.2	89.77	91.7	75.2	89.2	89.9	91.6	76.2	88.7	89.8	91.3	76.9	89.2	90.2	90.7	73.4
Cr#				9.3				8.8					7.3		16.6	
Sample	GX-9			GX-11			GX-12			GX-12						
Rock	Lherzolite			Lherzolite			Lherzolite			Lherzolite						
Mineral	OI	Opx	Cpx	Sp	OI	Opx	Cpx	Sp	OI	Opx	Cpx	Sp	Spongy Cpx-c	Spongy Cpx-m	Spongy Cpx-r	
Na ₂ O	—	0.03	0.60	—	0.01	0.03	1.03	0.01	0.01	0.14	1.76	—	1.83	1.76	0.68	

Table 3 continued

Sample	GX-9				GX-11				GX-12				GX-12			
	Lherzolite		Lherzolite		Lherzolite		Lherzolite		Lherzolite		Lherzolite		Lherzolite			
Rock	OI	Opx	Cpx	Sp	OI	Opx	Cpx	Sp	OI	Opx	Cpx	Sp	Spongy Cpx-c	Spongy Cpx-m	Spongy Cpx-r	
Mineral	MgO	47.48	32.57	15.89	18.66	47.87	32.28	14.91	18.73	49.92	33.61	15.93	18.27	15.66	15.46	16.74
	Al ₂ O ₃	-	3.70	4.50	52.90	0.01	3.66	4.95	54.97	0.01	3.94	5.52	50.30	5.71	5.73	4.59
	SiO ₂	40.14	55.68	53.58	0.07	40.94	55.59	51.94	0.02	40.87	55.18	53.56	0.07	52.83	52.19	52.49
	CaO	0.03	0.69	22.03	-	0.03	0.47	22.16	0.01	0.06	0.72	19.78	-	20.11	20.15	21.68
	TiO ₂	0.01	0.07	0.15	0.07	0.02	0.03	0.24	0.05	0.01	0.06	0.28	0.12	0.36	0.37	0.43
	Cr ₂ O ₃	0.02	0.35	0.84	15.84	0.02	0.35	0.86	13.30	0.04	0.47	1.07	19.07	1.30	1.38	1.33
	MnO	0.11	0.15	0.10	0.12	0.15	0.14	0.08	0.12	0.14	0.13	0.09	0.14	0.10	0.05	0.09
	FeO	9.95	6.19	2.45	11.49	9.58	6.21	2.32	11.75	9.19	5.90	2.80	12.19	2.87	2.77	2.96
	NiO	0.38	0.08	0.04	0.37	0.33	0.07	0.04	0.30	0.36	0.10	0.03	0.29	0.00	0.00	0.00
Total		98.12	99.51	100.16	99.53	98.97	98.83	98.53	99.28	100.60	100.27	100.82	100.47	100.76	99.86	100.98
Mg#		89.5	90.44	92.1	74.5	90.0	90.3	92.0	74.1	90.7	91.1	91.1	72.9	90.7	90.9	91.0
C#					16.7				14.0				20.3			
Sample	GX-14				GX-14				GX-15				GX-16			
Rock	Lherzolite		Lherzolite		Lherzolite		Lherzolite		Lherzolite		Lherzolite		Lherzolite			
Mineral	OI	Opx	Cpx	Sp	Spongy Cpx-c	Spongy Cpx-m	Spongy Cpx-r	OI	Opx	Cpx	Sp	OI	Opx	Cpx	Sp	
Na ₂ O	0.01	0.15	1.82	-	1.69	1.80	0.43	-	0.04	1.09	-	-	0.01	0.58	-	
MgO	48.84	33.03	15.64	20.16	15.44	15.52	16.76	49.37	33.72	15.27	19.84	49.62	34.44	16.39	17.36	
Al ₂ O ₃	0.03	4.65	6.61	57.01	6.50	6.71	4.57	0.01	3.58	5.59	58.98	0.01	2.62	3.40	48.82	
SiO ₂	40.57	55.31	52.78	0.06	51.45	51.50	50.24	40.87	56.08	53.48	0.01	40.77	56.15	53.16	0.05	
CaO	0.08	0.77	19.58	0.01	20.04	19.94	22.56	0.04	0.40	21.60	0.01	0.02	0.34	23.75	-	
TiO ₂	0.02	0.11	0.41	0.15	0.59	0.46	0.51	-	0.03	0.28	0.05	0.03	0.03	0.10	0.02	
Cr ₂ O ₃	0.03	0.40	0.77	12.06	0.81	0.89	1.10	0.04	0.29	0.88	11.06	0.03	0.30	0.71	20.49	
MnO	0.14	0.13	0.08	0.11	0.09	0.06	0.05	0.12	0.15	0.07	0.10	0.12	0.15	0.06	0.16	
FeO	9.56	6.09	2.95	11.06	3.01	2.95	2.75	10.16	6.59	2.41	10.87	9.43	6.32	2.13	13.33	
NiO	0.35	0.09	0.03	0.35	0.00	0.00	0.00	0.34	0.07	0.03	0.37	0.36	0.06	0.05	0.21	

Table 3 continued

Sample	GX-14				GX-14				GX-15				GX-16			
Rock	Lherzolite				Lherzolite				Lherzolite				Lherzolite			
Mineral	OI	Opx	Cpx	Sp	Spongy Cpx-c	Spongy Cpx-m	Spongy Cpx-r	OI	Opx	Cpx	Sp	OI	Opx	Cpx	Sp	
Total	99.63	100.74	100.66	100.96	99.62	99.87	98.96	100.94	100.95	100.69	101.30	100.40	100.43	100.34	100.45	
Mg#	90.2	90.7	90.5	76.6	90.1	90.4	91.6	89.7	90.18	91.9	76.6	90.4	90.7	93.3	70.1	
Cr#					12.4						11.2				22.0	
Sample	GX-19				GX-1				GX-6				GX-6			
Rock	Lherzolite				Harzburgite				Harzburgite				Harzburgite			
Mineral	OI	Opx	Cpx	Sp	OI	Opx	Cpx	Sp	OI-c	OI-m	OI-r		Opx-c	Opx-m	Opx-r	
Na ₂ O	—	0.04	1.08	0.01	—	—	0.19	—	—	—	—	0.10	0.04	0.04	0.04	
MgO	48.23	33.11	15.39	18.85	48.44	33.82	16.75	16.16	49.83	49.40	49.41	34.26	35.14	35.46		
Al ₂ O ₃	0.01	3.49	4.78	54.68	—	2.36	2.40	41.57	0.01	0.00	0.00	3.85	3.52	3.09		
SiO ₂	39.85	55.15	52.76	0.02	40.77	56.21	54.16	—	41.61	41.03	41.25	55.46	56.18	55.83		
CaO	0.03	0.46	22.24	—	0.02	0.45	23.72	0.01	0.02	0.04	0.02	0.94	0.42	0.45		
TiO ₂	0.01	0.06	0.22	0.07	—	0.02	0.08	0.09	0.17	—	—	0.02	0.05	0.05		
Cr ₂ O ₃	0.02	0.34	0.81	13.63	0.01	0.38	0.68	26.86	—	—	—	0.68	0.57	0.41		
MnO	0.12	0.15	0.07	0.12	0.12	0.14	0.07	0.16	0.14	0.16	0.11	0.18	0.14	0.10		
FeO	9.79	6.33	2.40	12.15	9.10	5.79	2.08	13.95	9.21	9.24	9.01	4.80	4.69	4.80		
NiO	0.35	0.06	0.03	0.31	0.41	0.06	0.04	0.18	0.41	0.39	0.34	0.08	0.15	0.14		
Total	98.40	99.18	99.78	99.84	98.87	99.22	100.18	98.98	101.40	100.26	100.15	100.38	100.91	100.39		
Mg#	89.8	90.4	92.0	73.6	90.5	91.3	93.5	67.5	90.7	90.6	90.8	92.8	93.1	93.0		
Cr#					14.3				30.2							
Sample	GX-6				GX-10				GX-13				GX-17			
Rock	Harzburgite				Harzburgite				Harzburgite				Harzburgite			
Mineral	Cpx-c	Cpx-m	Cpx-r	Sp	OI	Opx	Cpx	Sp	OI	Opx	Cpx	Sp	OI	Opx	Cpx	Sp
Na ₂ O	1.53	1.52	1.43	—	—	—	0.27	—	0.01	0.05	1.40	0.01	0.01	0.04	1.06	0.01
MgO	15.99	16.12	16.20	16.86	48.46	33.47	16.65	17.71	49.30	33.98	15.25	18.15	48.84	33.67	15.99	18.35
Al ₂ O ₃	5.17	5.16	4.59	43.53	—	2.46	2.43	48.53	—	3.10	4.64	48.37	0.02	2.93	3.95	47.20
SiO ₂	52.87	52.72	53.62	0.13	40.79	56.45	54.91	0.04	40.99	55.98	53.92	0.03	40.32	55.45	52.95	0.05
CaO	21.10	21.61	21.32	0.02	0.01	0.40	22.05	0.01	0.03	0.43	21.66	—	0.04	0.44	22.33	0.01

Table 3 continued

Sample	GX-6				GX-10				GX-13				GX-17			
	Harzburgite				Harzburgite				Harzburgite				Harzburgite			
Rock	Cpx-c	Cpx-m	Cpx-r	Sp	OI	Opx	Cpx	Sp	OI	Opx	Cpx	Sp	OI	Opx	Cpx	Sp
Mineral																
TiO ₂	0.26	0.22	0.25	0.10	–	0.02	0.09	0.04	0.01	0.05	0.16	0.07	–	0.04	0.08	0.06
Cr ₂ O ₃	1.50	1.52	1.31	25.36	–	0.29	0.58	21.00	0.02	0.38	1.11	20.51	0.03	0.36	0.91	20.89
MnO	0.08	0.08	0.04	0.16	0.13	0.13	0.07	0.15	0.12	0.14	0.06	0.15	0.11	0.13	0.07	0.12
FeO	1.77	1.92	1.64	13.12	9.43	5.99	2.10	11.72	8.65	5.63	2.06	11.54	8.86	5.72	2.13	11.82
NiO	0.04	0.06	0.06	0.23	0.39	0.09	0.04	0.27	0.36	0.08	0.03	0.24	0.33	0.08	0.03	0.17
Total	100.32	100.92	100.47	99.50	99.21	99.30	99.20	99.47	99.48	99.81	100.30	99.07	98.56	98.86	99.51	98.68
Mg#	94.2	93.8	94.7	69.8	90.2	90.9	93.4	73.1	91.1	91.6	93.0	73.9	90.8	91.4	93.1	73.6
C#				28.1		22.5						22.1				22.9
Sample	GX-18				GX-20				GX-21				GX-22			
Rock	Harzburgite				Harzburgite				Harzburgite				Harzburgite			
Mineral	OI	Opx	Cpx	Sp	OI	Opx	Cpx	Sp	OI	Opx	Cpx	Sp	OI	Opx	Cpx	Sp
Na ₂ O	–	0.03	1.24	0.01	0.01	0.05	1.17	–	0.01	0.08	0.91	–				
MgO	49.00	33.88	15.50	18.15	49.69	34.02	15.57	18.46	48.75	33.50	17.43	14.84				
Al ₂ O ₃	0.03	2.97	4.63	48.17	0.01	3.27	4.59	48.45	0.04	2.46	2.60	28.95				
SiO ₂	40.47	55.49	52.99	0.03	40.18	55.91	52.98	0.15	40.21	55.70	54.00	0.06				
CaO	0.02	0.43	22.32	0.01	0.04	0.51	22.18	0.01	0.07	0.86	20.83	0.03				
TiO ₂	0.01	0.03	0.10	0.06	0.01	0.07	0.22	0.12	0.01	0.01	0.02	0.01				
Cr ₂ O ₃	0.06	0.37	1.13	20.45	0.01	0.44	1.08	21.49	0.05	0.66	0.84	40.33				
MnO	0.11	0.14	0.07	0.15	0.13	0.13	0.08	0.14	0.13	0.14	0.09	0.21				
FeO	8.94	5.81	2.09	11.61	9.28	5.83	2.26	11.47	8.98	5.47	2.59	14.28				
NiO	0.31	0.08	0.04	0.26	0.35	0.09	0.04	0.29	0.34	0.10	0.05	0.18				
Total	98.96	99.22	100.11	98.88	99.70	100.31	100.16	100.57	98.60	98.97	99.37	98.89				
Mg#	90.8	91.29	93.0	73.7	90.6	91.3	92.5	74.3	90.7	91.7	92.4	65.1				
C#				22.2					22.9			48.3				

OI olivine, Opx orthopyroxene, Cpx clinopyroxene, Sp spinel, c core, m mantle, r rim; Mg#=100 × molar Mg/(Mg+Fe); Cr#=100 × molar Cr/(Cr+Al)

– Below detection limit

Table 4 Trace element abundances of clinopyroxene separates from Shangzhi peridotite xenoliths

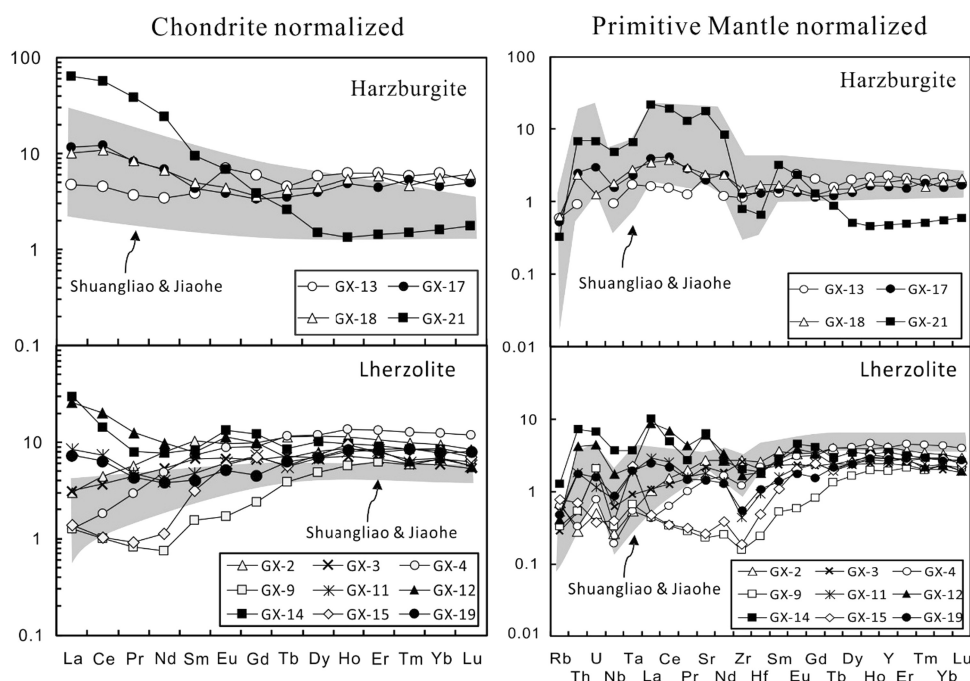
Rock type Sample	Lherzolite										Harzburgite			
	GX-2	GX-3	GX-4	GX-9	GX-11	GX-12	GX-14	GX-15	GX-19	GX-13	GX-17	GX-18	GX-21	
Sc	54.9	55.6	64.5	61.2	59.1	55.5	48.9	59.5	59.6	52.7	62.8	63.7	53.8	
V	244	217	262	246	194	188	180	201	175	181	160	171	144	
Cr	4458	3973	3956	4592	2033	2948	1976	1863	1750	2214	2000	2610	1890	
Co	29.7	29.7	31.7	41.4	34.4	28.7	38.2	34.5	29.8	38.2	42.9	39.2	44.9	
Ni	532	510	530	664	461	381	508	471	387	508	587	533	567	
Rb	0.45	0.18	0.41	0.21	0.34	0.27	0.83	0.49	0.30	0.37	0.34	0.39	0.21	
Th	0.02	0.04	0.03	0.05	0.16	0.36	0.62	0.06	0.15	0.08	0.21	0.20	0.58	
U	0.01	0.05	0.02	0.04	0.02	0.09	0.14	0.01	0.03	0.00	0.06	0.03	0.15	
Nb	0.19	0.45	0.14	0.23	0.56	1.25	2.64	0.28	0.63	0.66	1.12	1.30	3.45	
Ta	0.02	0.04	0.02	0.03	0.08	0.09	0.15	0.09	0.08	0.07	0.10	0.12	0.28	
La	0.71	0.75	0.30	0.30	1.99	6.11	7.16	0.33	1.72	1.12	2.76	2.38	15.20	
Ce	2.74	2.25	1.12	0.61	4.51	12.40	8.78	0.63	3.89	2.77	7.38	6.63	34.70	
Pr	0.55	0.42	0.28	0.08	0.45	1.20	0.76	0.09	0.41	0.35	0.78	0.81	3.62	
Sr	57	46	31	5	37	128	137	6	30	45	42	51	377	
Nd	3.67	2.50	2.26	0.35	1.85	4.59	3.62	0.52	1.77	1.60	3.21	3.15	11.40	
Zr	30.40	29.10	13.60	1.74	4.94	18.90	23.00	2.10	6.13	12.60	14.34	16.90	9.00	
Hf	0.79	0.62	0.68	0.08	0.29	0.57	0.58	0.15	0.34	0.45	0.40	0.53	0.20	
Sm	1.59	1.03	1.11	0.24	0.72	1.20	1.28	0.48	0.62	0.58	0.66	0.76	1.43	
Eu	0.57	0.40	0.51	0.10	0.36	0.66	0.77	0.34	0.30	0.40	0.22	0.25	0.39	
Gd	2.02	1.35	1.87	0.49	1.48	2.03	2.50	1.45	0.93	1.22	0.69	0.74	0.78	
Tb	0.43	0.27	0.44	0.15	0.21	0.25	0.32	0.21	0.23	0.17	0.13	0.16	0.10	
Dy	2.92	1.73	3.00	1.23	1.73	2.02	2.58	1.86	1.78	1.46	1.00	1.12	0.38	
Ho	0.64	0.40	0.77	0.33	0.46	0.49	0.55	0.53	0.48	0.36	0.27	0.31	0.07	
Y	18.90	11.10	18.90	8.72	11.90	13.20	16.10	13.70	12.90	10.40	7.34	8.40	2.18	
Er	1.76	1.11	2.19	1.04	1.36	1.29	1.52	1.31	1.38	1.02	0.73	0.96	0.24	
Tm	0.25	0.15	0.33	0.15	0.15	0.17	0.22	0.21	0.22	0.15	0.14	0.12	0.04	
Yb	1.60	1.00	2.11	1.13	1.13	1.17	1.45	1.40	1.32	1.07	0.76	0.94	0.27	
Lu	0.22	0.14	0.30	0.16	0.14	0.14	0.19	0.18	0.20	0.13	0.13	0.16	0.04	

Rock type Sample	Standard			Standard		
	This study		Recommended value	This study		Recommended value
	Basalt	BHVO-2		Basalt	BHVO-2	
Sc	32.3		32.0		13.4	13.0
V	334		317		123	120
Cr	243		280		17	17
Co	46.0		45.0		15.9	16.0
Ni	109		119		20	19
Rb	9.22		9.11		66.70	68.60
Th	1.18		1.22		5.98	6.10
U	0.43		0.40		1.84	1.88
Nb	18.60		18.10		15.30	15.00
Ta	1.19		1.14		0.91	0.89
La	15.50		15.20		37.60	38.00
Ce	38.20		37.50		68.20	68.00
Pr	5.44		5.35		7.99	8.30
Sr	401		396		661	658

Table 4 continued

Rock type Sample	Standard		Standard	
	This study	Recommended value	This study	Recommended value
	Basalt BHVO-2	Basalt BHVO-2	Andesite AGV-2	Andesite AGV-2
Nd	24.60	24.50	30.90	30.00
Zr	171.00	172.00	228.00	230.00
Hf	4.41	4.36	5.70	5.08
Sm	6.16	6.07	5.62	5.70
Eu	2.09	2.07	1.58	1.54
Gd	6.27	6.24	4.88	4.69
Tb	0.96	0.92	0.67	0.64
Dy	5.30	5.31	3.41	3.60
Ho	1.01	0.98	0.67	0.71
Y	24.60	26.00	18.50	20.00
Er	2.57	2.54	1.81	1.79
Tm	0.34	0.33	0.24	0.26
Yb	2.00	2.00	1.59	1.60
Lu	0.28	0.27	0.23	0.25

Fig. 4 Chondrite-normalized REE patterns **a, c** and primitive mantle-normalized incompatible element patterns **b, d** for Cpx from the Shangzhi peridotite xenoliths. Chondrite normalization values are from Anders and Grevesse (1989). Primitive mantle normalization values are from McDonough and Sun (1995). Cpx in the Jiaohe and Shuangliao lherzolites and harzburgites reported by Yu et al. 2009 are also shown for comparison



2017b). The $\delta^7\text{Li}$ values of olivine range from 0.3‰ to 8.1‰ and these values are much higher than the coexisting Cpx ($-13.8\text{\textperthousand}$ to $+7.7\text{\textperthousand}$) (Table 5; Fig. 5d). Moreover, the Li contents of olivine tend to decrease with increasing modal olivine, which is consistent with the melt depletion trend (Fig. 5e, Rudnick and Ionov 2007; Xiao et al. 2017). The $\delta^7\text{Li}$ values of olivine tend to decrease with increasing

forsterite content (Fo) (Fig. 5f). There are roughly negative correlations between whole rock MgO contents and Li concentrations (Fig. 6a) and $\delta^7\text{Li}$ values for olivine (Fig. 6b). However, no correlation exists for Cpx in Shangzhi xenoliths (Fig. 6a, b). Moreover, minerals in “depleted” samples [$(\text{La}/\text{Sm})_n < 1$] show similar ranges of Li concentrations and $\delta^7\text{Li}$ values compared with

Table 5 Li concentration and isotopic compositions from Shangzhi peridotite xenoliths

Sample	Olivine			Cpx			Reconstructed bulk		$D_{Li}^{ol/cpx}$	Δ^7Li_{ol-cpx}
	Li (ppm)	δ^7Li	2SD	Li (ppm)	δ^7Li	2SD	Li (ppm)	δ^7Li		
<i>Lherzolite</i>										
GX-2	2.70	3.00	0.13	2.26	– 8.01	0.14	2.46	– 1.58	1.20	11.01
GX-3	1.24	5.56	0.08	1.14	1.29	0.14	1.19	4.47	1.09	4.27
GX-4	1.63	4.97	0.13	2.00	– 3.68	0.19	1.71	1.40	0.82	8.65
GX-9	0.93	8.09	0.19	3.79	– 13.76	0.17	1.84	1.02	0.25	21.85
GX-11	0.68	3.20	0.14	1.40	– 2.31	0.14	0.90	1.32	0.48	5.51
GX-12	1.73	6.38	0.08	6.11	– 9.09	0.14	3.22	1.12	0.28	15.47
GX-14	1.93	5.80	0.17	3.82	– 10.18	0.13	2.61	– 0.61	0.51	15.98
GX-15	1.26	5.53	0.08	4.09	– 5.96	0.17	2.37	0.60	0.31	11.49
GX-19	1.78	5.00	0.14	1.50	– 12.46	0.13	1.65	– 1.21	1.19	17.46
<i>Harzburgite</i>										
GX-13	0.29	1.44	0.17	4.42	– 5.77	0.13	0.99	0.19	0.07	7.21
GX-17	1.23	2.27	0.14	2.52	– 1.92	0.17	1.36	1.78	0.49	4.19
GX-18	0.96	0.33	0.17	1.99		0.13	1.05	0.30	0.48	
GX-21	0.90	2.67	0.17	0.89	7.68	0.17	0.88	3.77	1.01	– 5.01
International rock standard			Description			δ^7Li			References	
BHVO-2			Basalt			4.04 ± 0.14			This study	
						4.1 ± 0.2			Krienitz et al. (2012)	
						4.2 ± 0.5			Vlastélic et al. (2011)	
						$+ 4.4 \pm 0.3$			Sun et al. (2016)	
GSP-2			Granodiorite			$- 0.89 \pm 0.14$			This study	
						$- 0.79 \pm 0.3$			Lin et al. (2016)	
						$- 0.74 \pm 0.2$			Simons et al. (2010)	
						$- 0.8 \pm 0.3$			Sun et al. (2016)	

Ol olivine, *Cpx* clinopyroxene, Bulk reconstructed δ^7Li calculated using modal composition in Table 1 (the Opx is assumed to have the same δ^7Li as the Cpx)

$D_{Li}^{ol/cpx}$: partition coefficient for Li between olivine and Cpx

Δ^7Li_{ol-cpx} : Li isotope fractionation between olivine and Cpx

those in “metasomatised” samples [$(La/Sm)_n$ in Cpx > 1, Fig. 6c, d].

5 Discussion

5.1 Partial melting and metasomatism in the Shangzhi peridotite xenoliths

The Shangzhi peridotites delineate a sequence from primitive lherzolite through Cpx-poor lherzolite to highly refractory harzburgite. These peridotites define a correlation between Mg#_{ol} and Cr#_{sp} (Fig. 3c), which is in accordance with experimental data (Jaques and Green 1980) and studies on natural samples (Cabanes and Mercier 1988). Specifically, Shangzhi lherzolites show low and

restricted variation of Mg#_{ol} (88.75–90.70) similar to the fertile normal-mantle peridotite, indicating low degrees of partial melting. Refractory harzburgites show high and restricted Mg#_{ol} (90.23–91.10) corresponding to high degrees of partial melting. These observations are consistent with whole rock major element compositions (Fig. 3a). For instance, in the diagram of MgO versus Al₂O₃, the Shangzhi peridotites follow the modeled partial melting trend of Niu (1997). Modeling the behavior of immobile elements during fractional melting within the spinel stability field (Johnson et al. 1990; Norman 1998) suggests that the Shangzhi lherzolites are residues generated by relatively lower degrees of partial melting (< 7%), whereas the Shangzhi harzburgites were formed through higher degrees of partial melting (8%–18%).

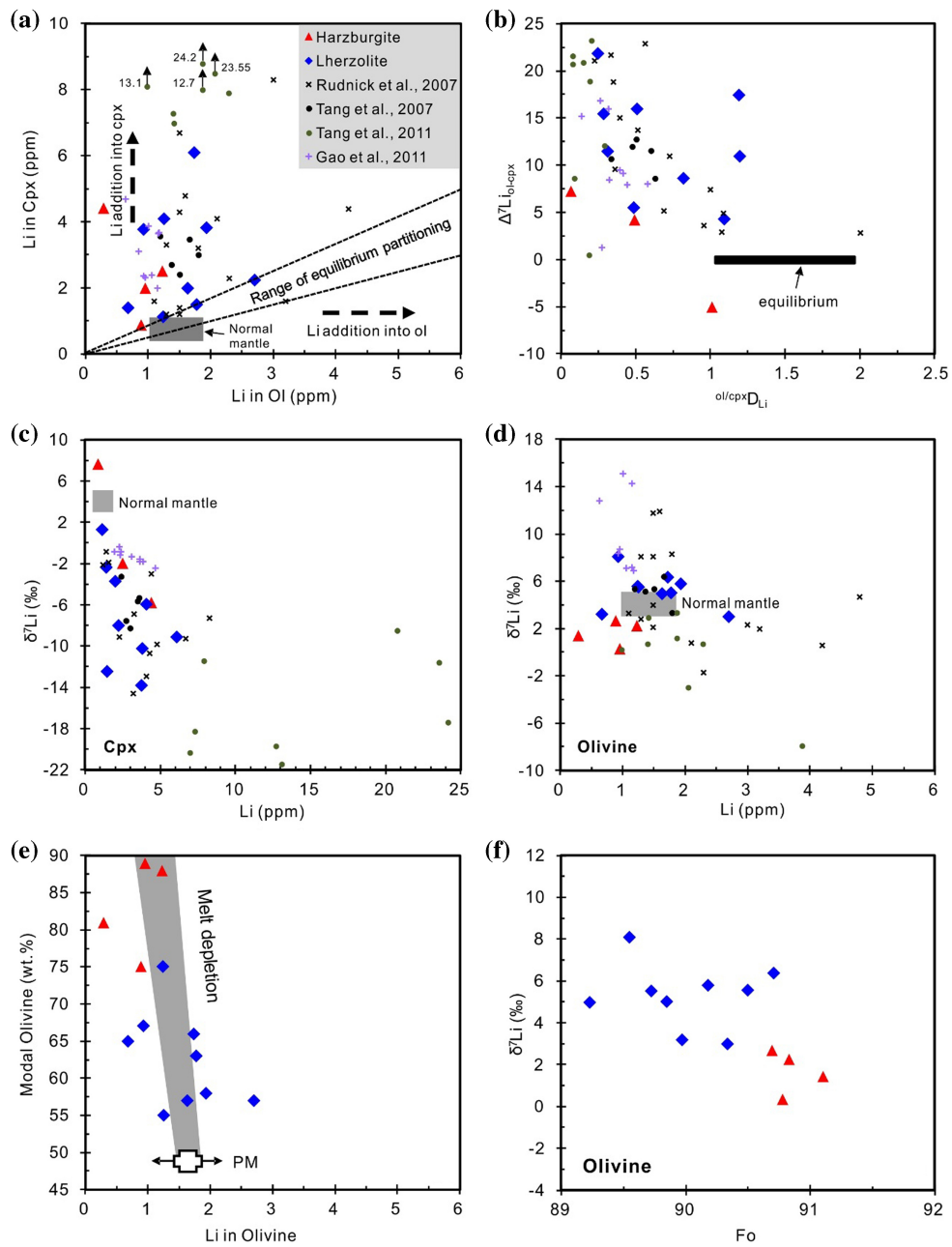
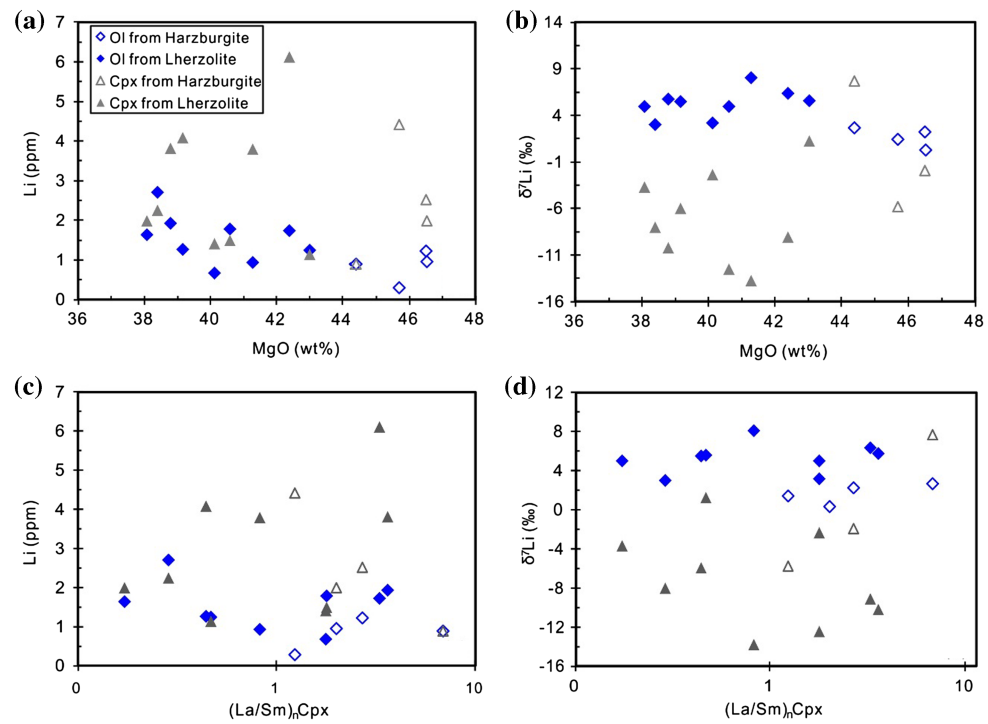


Fig. 5 **a** Lithium abundance in Cpx versus coexisting olivine; **b** plot of partition coefficient for Li between olivine and Cpx ($\text{ol}/\text{cpx} D_{\text{Li}}$) versus Li isotopic fractionation between olivine and Cpx ($\Delta^7\text{Li}_{\text{ol}-\text{cpx}}$). Gray horizontal bar shows equilibrium conditions from Rudnick and Ionov (2007) with equilibrium $\Delta^7\text{Li}_{\text{ol}-\text{cpx}}$ assumed here to be zero ($\pm 1\text{‰}$) at mantle temperature; **c–d** plots of Li concentration against $\delta^7\text{Li}$ for olivine and Cpx. Grey field for “normal mantle” in (a) is represented by fertile to moderately depleted peridotites (Seitz and Woodland 2000). The range of equilibrium partitioning of Li between olivine and Cpx are from Brenan et al. (1998), Eggins et al. (1998) and Seitz and Woodland (2000) ($\text{ol}/\text{cpx} D_{\text{Li}} = 1.1\text{--}2.0$). Grey fields in (c) and (d) are after Jeffcoate et al. (2007), Pogge von Strandmann et al. (2011) and Lai et al. (2015). Peridotitic samples from Rudnick and Ionov (2007), Tang et al. (2007b, 2011) and Gao and Snow (2011) are shown for comparison; **e** plot of modal olivine against Li concentration in olivine. Melt depletion trend is after Rudnick and Ionov (2007). Primitive mantle (PM) is after Sun and McDonough (1989); **f** plot of Fo against $\delta^7\text{Li}$ (‰) in olivine

Most Shangzhi peridotites show signs of mantle metasomatism, such as enrichment in Na_2O (Fig. 3b, d) and highly incompatible elements (e.g., Th, U, Nb, LREE; Fig. 4). Cpx in two lherzolites, i.e. GX-9 and GX-15, displays a spoon-shaped REE pattern, resembling the Cpx

with analogous shapes and enrichment in mantle peridotites from Shuangliao and Jiaohe in NE China (Fig. 4; Yu et al. 2009), which can be explained by the chromatographic metasomatism of melt infiltration (Navon and Stolper, 1987). Cpx in harzburgites overall displays

Fig. 6 a–b Plots of whole-rock MgO against Li concentration and $\delta^7\text{Li}$ in olivine and Cpx; c–d plots of primitive mantle normalized La/Sm ratios in Cpx versus Li concentration and $\delta^7\text{Li}$ in olivine and Cpx



enriched-LREE patterns. It should be pointed out that Cpx in harzburgite GX-21 has remarkably higher LREE and LILE enrichment than other peridotites (Fig. 4), which suggests that this sample has experienced stronger mantle metasomatism compared with other samples. The absence of modal metasomatic minerals (i.e., mica, amphibole or apatite) suggests that the metasomatism that was responsible for the enrichment of incompatible elements in the Shangzhi peridotites is largely cryptic, i.e., only introducing incompatible elements without any petrographic modification (Frey and Green 1974). It remains to assess whether the enrichment of incompatible elements in the Shangzhi peridotites was related to chromatographic metasomatism with a single agent, or multiple metasomatism involving different metasomatic agents. It has been suggested that mantle xenoliths metasomatized by silicate melt would be enriched in incompatible trace elements including Th, U, Nb, and LREE (e.g., Wittig et al. 2007; Neumann and Wulff-pedersen 1997). In contrast, percolating of the other kinds of melts, such as volatile-rich or carbonatite melts may only result in LILE enrichment, while their HFSE (e.g., Ti and Zr) concentrations were little changed (e.g., Ionov et al. 1996; Yaxley et al. 1991; O'Reilly and Griffin 1988). Cpx in the Shangzhi peridotite xenoliths have low $(\text{La/Yb})_h$ but highly variable Ti/Eu ratios, plotting within the field of silicate metasomatism (Fig. 7). This suggests that the Shangzhi peridotites have been subjected to silicate metasomatism.

5.2 Origin of Li isotopic fractionation in the Shangzhi peridotite xenoliths

5.2.1 Equilibrium fractionation during partial melting

Li concentration (0.3–2.7 ppm) of olivine from the Shangzhi peridotites are similar to the normal mantle (1–1.8 ppm; Seitz and Woodland 2000; Fig. 5a) and show roughly negative correlations with the indices of melt extraction (such as modal olivine and whole rock MgO) (Figs. 5e, 6a). These features are consistent with variable degrees of partial melting because Li is a moderately incompatible element whose partition coefficient remains constant as long as equilibrium is maintained. Partial melting of mantle peridotite can lead to Li depletion of < 1 ppm in olivine (Xiao et al. 2017). On the other hand, $\delta^7\text{Li}$ values for olivine (mostly ranging from 2‰ to 6‰) in the Shangzhi peridotites are comparable to the estimated isotopic composition of the normal mantle (3‰ to 5‰) (Magna et al. 2008; Pogge von Strandmann et al. 2011; Lai et al. 2015). $\delta^7\text{Li}$ values for olivine are also negatively correlated with Fo (Fig. 5f) and whole rock MgO (Fig. 6b). This feature can also be attributed to variable degrees of partial melting (Xiao et al. 2017).

Coexisting Cpx displays variable degrees of Li enrichment (0.9–6.1 ppm) and extremely low $\delta^7\text{Li}$ values (−13.8‰ to +7.7‰) compared with the normal mantle (Fig. 5c). Moreover, in the diagram of the partition coefficient for Li between olivine and Cpx ($D_{\text{Li}}^{\text{ol/cpx}}$) versus the

degree of isotopic equilibrium ($\Delta^7\text{Li}_{\text{ol}/\text{cpx}}$, Fig. 5b), the Shangzhi peridotites display strong element and isotopic disequilibria. Such characteristics clearly cannot be explained by equilibrium fractionation during partial melting and may reflect later Li addition to Cpx after the partial melting events.

5.2.2 The effect of diffusive fractionation on minerals in the Shangzhi peridotite xenoliths

Diffusion is an important mechanism for the Li isotopic variation in mantle peridotites (Tomasca et al. 2016). Various diffusion processes have been proposed to account for Li isotopic variations in mantle xenoliths, including Li-redistribution between minerals during slow cooling of xenoliths after the eruption of their host magmas (Ionov and Seitz 2008; Gallagher and Elliott 2009; Gao and Snow 2011), lithium addition from recycled melt with low $\delta^7\text{Li}$ (Nishio et al. 2004; Tang et al. 2007b, 2012, 2014; Su et al. 2016) and Li diffusion from host magma/percolating melt (Rudnick and Ionov 2007; Jeffcoate et al. 2007; Aulbach et al. 2008, 2013; Aulbach and Rudnick 2009; Lai et al. 2015). These possibilities are evaluated below.

Gallagher and Elliott (2009) proposed a model that describes diffusion of Li from olivine into Cpx related to slow cooling of xenoliths after the eruption of their host magmas. In this model, $\delta^7\text{Li}$ for Cpx tends to be lower, while $\delta^7\text{Li}$ for olivine tends to be higher than the normal mantle due to faster diffusion of ${}^6\text{Li}$ than ${}^7\text{Li}$ from olivine to Cpx during slow cooling of the magmatic system (Fig. 5c, d; Ionov and Seitz 2008; Gao and Snow 2011). Meanwhile, Li concentrations of Cpx tend to be higher,

while Li concentrations of olivine tend to be lower than the normal mantle during cooling. However, olivine in the Shangzhi peridotites shows generally normal mantle-like $\delta^7\text{Li}$ and Li concentrations (Fig. 5d) (Magna et al. 2008; Pogge von Strandmann et al. 2011; Lai et al. 2015), which is inconsistent with this model. Moreover, Li isotopic fractionation between minerals during slow cooling of a magmatic system typically displays increasing $\Delta^7\text{Li}_{\text{ol}-\text{cpx}}$ ($\delta^7\text{Li}_{\text{ol}}-\delta^7\text{Li}_{\text{cpx}}$) values with decreasing temperature (Gao and Snow 2011). However, such a phenomenon was not observed in the Shangzhi peridotites. More direct evidence is from the reconstructed bulk $\delta^7\text{Li}$ and Li concentrations of the Shangzhi peridotites (Table 5) which show higher Li concentration (0.9–3.2 ppm) and lower $\delta^7\text{Li}$ (−1.6‰ to +4.5‰) than the normal mantle (1–1.5 ppm and 3‰–5‰) (Seitz and Woodland 2000; Magna et al. 2008; Pogge von Strandmann et al. 2011; Lai et al. 2015). This clearly cannot be explained by redistribution of Li during slow cooling of a magmatic system because such closed-system Li-redistribution would only cause transitory fractionations of Li isotopes between coexisting minerals. The bulk Li isotopic compositions should remain unchanged. Thus, all these features are inconsistent with the model of Li isotopic fractionation during slow cooling.

Low $\delta^7\text{Li}$ melt/fluid related to subducted slab has been invoked to explain the negative $\delta^7\text{Li}$ values observed in Cpx separated from mantle xenoliths (Nishio et al. 2004; Tang et al. 2007b, 2012, 2014; Su et al. 2012, 2014a). High Li concentrations and negative $\delta^7\text{Li}$ values for Cpx from the Shangzhi peridotites apparently can be attributed to subduction-related melt infiltration. Moreover, low bulk $\delta^7\text{Li}$ (−1.6‰ to +4.5‰) and high bulk Li concentrations (0.9–3.2 ppm) of the Shangzhi peridotites are also consistent with low- $\delta^7\text{Li}$ melt/fluid addition. The possible role of low- $\delta^7\text{Li}$ melt addition in the genesis of the Shangzhi peridotites can be evaluated by mixing calculations using Li concentration and $\delta^7\text{Li}$ values (Fig. 8). We use Cpx from normal mantle with $\delta^7\text{Li}$ of 3.5‰ and Li concentration of 1 ppm to represent the composition of Cpx from uncontaminated mantle peridotite (Seitz and Woodland 2000; Magna et al. 2008; Pogge von Strandmann et al. 2011; Lai et al. 2015). The $\delta^7\text{Li}$ values for assumed infiltrated melt/fluid range from −20‰ to −10‰, which is similar to the values of subduction-related eclogites (Zack et al. 2003; Marschall et al. 2007; Halama et al. 2011). The Li concentration of subduction-related melt/fluid is assumed to be 50 ppm. The high Li concentrations of these melts/fluids were generated by the variable degrees of partial melting which fall within the range of Li concentrations of arc lavas (7–53 ppm) (Chan et al. 2002; Agostini et al. 2008; Tang et al. 2014). The results show that variations of Li concentrations and $\delta^7\text{Li}$ values for Cpx from the Shangzhi peridotites require addition of up to

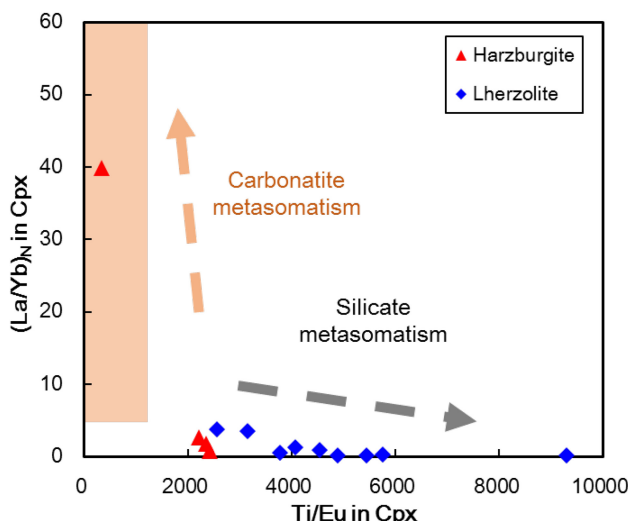


Fig. 7 Plots of Ti/Eu against $(\text{La}/\text{Yb})_{\text{N}}$ in Cpx from the Shangzhi peridotites. Field for “silicate” and “carbonatitic” metasomatism are after Coltorti et al. (1999)

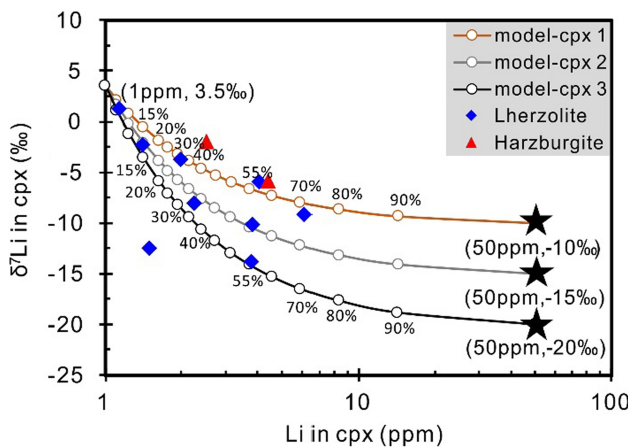


Fig. 8 Binary mixing of Cpx of variable degrees by assumed subduction-related melts with low $\delta^7\text{Li}$ values ($-10\text{\textperthousand}$ to $-20\text{\textperthousand}$). See text for more detailed explanation

50%–60% of melt/fluid derived from subduction oceanic crust (Fig. 8). Such large quantities of melt addition are unrealistic and would not retain a peridotitic composition. Moreover, the $\delta^7\text{Li}$ for olivine should be also low if the low $\delta^7\text{Li}$ for Cpx was the effect of low- $\delta^7\text{Li}$ melt infiltration. On the other hand, Li concentration of olivine should be higher than the normal mantle because of external Li addition. These features are inconsistent with olivine in the Shangzhi peridotites which show generally normal mantle-like $\delta^7\text{Li}$ and Li concentrations (Fig. 5d). Thus, this possibility is short of strong evidence although it cannot be totally ruled out.

We consider that the low $\delta^7\text{Li}$ and high Li contents for Cpx and some bulk peridotites from Shangzhi were generated by kinetic isotope fractionation due to Li diffusion from host magma/percolating melt/fluid shortly before or coincident with their entrainment into the host magmas (Jeffcoate et al. 2007; Rudnick and Ionov 2007; Aulbach

et al. 2008; Magna et al. 2008; Su et al. 2014b). This percolating melt/fluid would generate a chemical potential gradient to drive diffusion of Li from melt into peridotite. ${}^6\text{Li}$ would preferentially diffuse out of melt conduits into wall-rock peridotites during this process (Lundstrom et al. 2005) and result in the decreasing of $\delta^7\text{Li}$ for Cpx and bulk peridotite from Shangzhi. At the same time, low Li concentrations and normal mantle-like isotopic compositions of olivine in the Shangzhi samples suggest olivine was little affected by external Li addition. This may relate to much lower diffusivity of Li in olivine and larger grain sizes of olivine relative to Cpx (Richter et al. 2003, 2014).

In order to quantify how Li isotope ratios and concentrations change due to chemical diffusion from the percolating melt/fluid, we conduct a modeling calculation applying the equation from Lai et al. (2015):

$$C(t) = Cr + \frac{6(Ci - Cr)}{\pi^2} \sum_{n=1}^{\infty} \frac{1}{n^2} \exp\left(\frac{-Dtn^2\pi^2}{a^2}\right)$$

In this equation, “ $C(t)$ ” represents the Li concentration in a bulk mineral at a given time; “ Ci ” represents the original concentration in the mineral core; “ Cr ” represents the Li concentration at the mineral surface, which is in equilibrium with the percolating melt; “ D ” represents the diffusion coefficient of Li in a mineral; “ t ” represents time and “ a ” represents the radius of a mineral. We assume that the crystal is a sphere and the grain radius is “ r ”. We also assume the melt-rock interaction occurred at 1200 °C and remained constant over the relatively short period of melt percolation. Li diffusivities in Cpx and olivine at 1200 °C are 2.1×10^{-11} and 2.29×10^{-15} m²/s, respectively (Coogan et al. 2005; Dohmen et al. 2010). The partition coefficient of Li in Cpx and olivine are 0.27 and 0.35, respectively (Brenan et al. 1998). The diffusion coefficients of both ${}^6\text{Li}$ and ${}^7\text{Li}$ are related by the expression $D_7/D_6 = (m_6/m_7)^\beta$, where m_6 and m_7 are atomic masses (i.e., 6

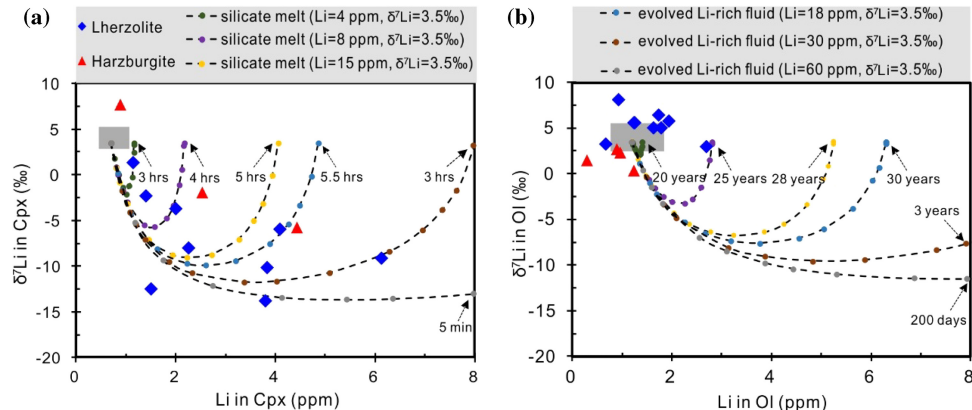


Fig. 9 Modeled trajectories of Li concentrations against $\delta^7\text{Li}$ for Cpx **a** and olivine **b** experiencing Li diffusion from silicate melts or Li-rich fluids with normal mantle-like $\delta^7\text{Li}$ and variable Li concentrations. Each curve represents the pathway of a mineral with elapsed time. Grey fields show range of “normal mantle” concentrations and $\delta^7\text{Li}$ for Cpx and olivine. See text for more detailed explanation

and 7) (Richter et al. 2003). A value for β of 0.27 is used in this model (Richter et al. 2014). The grain radiuses are 0.5 mm for Cpx and 1.5 mm for olivine, respectively.

The initial Li concentration and $\delta^7\text{Li}$ for Cpx are assumed to be 0.7 ppm and 3.5‰, respectively, which are within the range of normal mantle (Seitz and Woodland 2000; Magna et al. 2008; Pogge von Strandmann et al. 2011; Lai et al. 2015). The initial Li concentration and $\delta^7\text{Li}$ for olivine are assumed to be 1.2 ppm and 3.5‰, respectively, which are within the range of pristine upper mantle values (Seitz and Woodland 2000; Magna et al. 2008; Pogge von Strandmann et al. 2011; Lai et al. 2015). Silicate melt and fluid are used in our calculation. As discussed earlier, incompatible trace element enrichment in Cpx is possibly related to silicate melt metasomatism. It is reasonable to speculate that a possible relationship exists between Li isotope fractionation and silicate melt infiltration. The Li isotope composition of these percolating melts is speculated to be the same as that of common mantle melts (3.5‰). Li concentrations of silicate melts are assumed to be ranging from 4 to 15 ppm, which are similar to those of typical MORB and OIB (Chan and Frey 2003; Elliott et al. 2006; Tomascak et al. 2008; Magna et al. 2008; Marschall et al. 2017). Li concentrations of fluids (18–60 ppm) are speculated to be much higher than typical silicate melts (Wunder et al. 2006). These fluids may come from degassing and the fractional crystallization of the magma due to the high solubility of Li in fluids (Rudnick and Ionov 2007) or from exsolution of Li-rich fluids from the magma due to a high partition coefficient between fluid and melt ($D^{\text{Li}}_{\text{fluid/melt}}$ up to 13) (Webster et al. 1989) during exsolution of a chlorite-bearing fluid (Teng et al. 2006; Aulbach and Rudnick 2009; Schuessler et al. 2009).

The calculated results show that Li diffusion from silicate melts or Li-rich fluids leads to a strong enrichment of Li and a sharp decrease of $\delta^7\text{Li}$ for Cpx in a very short time (several minutes to ~ 5 h, Fig. 9a). In contrast, it would take much more time to lower $\delta^7\text{Li}$ for olivine (several years, Fig. 9b). The low $\delta^7\text{Li}$ and high Li contents of Cpx from the Shangzhi peridotites can be readily explained by Li diffusion from silicate melts or Li-rich fluids in a very recent time (Fig. 9a). The Cpx with light $\delta^7\text{Li}$ values and Li enrichment is also observed in a suite of spinel peridotites from Hannuoba, Fanshi, Hebi areas in the North China Craton (NCC), which was explained to be a consequence of diffusive fractionation caused by recent Li ingress from infiltrating melts/fluids (Tang et al. 2007b, 2011). Compared to the published Li isotopic data of bulk minerals from NCC, Cpx in the Shangzhi peridotites shows similar variations in Li abundances and $\delta^7\text{Li}$ (Fig. 5c, d). Furthermore, in situ isotopic profiles across minerals from Hannuoba, Beiyuan, Kuandian xenoliths from

NCC, and Dayishan xenoliths from NE China revealed clear Li isotopic zoning in Cpx, displaying increasing Li concentration and decreasing $\delta^7\text{Li}$ from core to rim, which can be attributed to Li diffusive ingress into Cpx from metasomatic melts/fluids (Tang et al. 2007b; Xu et al. 2013a, b; Xiao et al. 2015; Su et al. 2017b). Thus, these observations provide further evidence that diffusive fractionation of Li isotopes during peridotite-melt/fluid interaction plays an important role in producing Li enrichment and light $\delta^7\text{Li}$ of Cpx in the Shangzhi peridotites. On the other hand, normal mantle-like isotopic compositions and low Li concentrations of olivine from the Shangzhi peridotites imply that olivine was little affected by such short-time melt/fluid infiltration because of much lower diffusivity of Li in olivine (Richter et al. 2003, 2014). Lastly, the light Li isotopic compositions preserved in the bulk samples also indicate that the percolated melts/fluids have not had enough time to isotopically equilibrate with the bulk peridotite.

6 Conclusions

Li isotopic fractionation in the Shangzhi mantle xenoliths is mainly related to Li diffusion from silicate melts or Li-rich fluids shortly before or coincident with their entrainment into the host magmas. Low $\delta^7\text{Li}$ and high Li contents of Cpx from the Shangzhi peridotites can be explained by Li diffusion from such melts/fluids in a very short time (several minutes to several hours). In contrast, normal mantle-like isotopic compositions and low Li concentrations of olivine from the Shangzhi peridotites indicate that olivine was little affected by such short-time melts/fluids infiltration. The negative correlation between $\delta^7\text{Li}$ and Fo for olivine is consistent with variable degrees of partial melting rather than melt infiltration.

Acknowledgements We thank Prof. Yi-Lin Xiao and Hai-Yang Liu from the University of Science and Technology of China and Ting Zhou from the Institute of Geochemistry, Chinese Academy of Sciences for their assistance in analysis of Li isotopes. This study was funded by the strategic priority research program (B) of the Chinese Academy of Sciences (XDB18000000), NSFC (41573009; 41373042, 41203031). Open research fund of the State Key Laboratory of Ore Deposit Geochemistry of China (SKLOGD Grant # 201204). We thank three anonymous reviewers for their constructive reviews which greatly improved the quality of this manuscript.

References

- Ackerman L, Špaček P, Magna T, Ulrych J, Svojtka M, Hegner E, Balogh K (2013) Alkaline and carbonate-rich melt metasomatism and melting of subcontinental lithospheric mantle: evidence from mantle xenoliths, NE Bavaria, Bohemian Massif. *J Petrol* 54:2597–2633

- Agostini S, Ryan JG, Tonarini S, Innocenti F (2008) Drying and dying of a subducted slab: coupled Li and B isotope variations in Western Anatolia Cenozoic Volcanism. *Earth Planet Sci Lett* 272:139–147
- Anders E, Grevesse N (1989) Abundances of the elements: meteoritic and solar. *Geochim Cosmochim Acta* 53:197–214
- Aulbach S, Rudnick RL (2009) Origins of non-equilibrium lithium isotopic fractionation in xenolithic peridotite minerals: examples from Tanzania. *Chem Geol* 258:17–27
- Aulbach S, Rudnick RL, McDonough WF (2008) Li–Sr–Nd isotope signatures of the plume and cratonic lithospheric mantle beneath the margin of the rifted Tanzanian craton (Labait). *Contrib Mineral Petrol* 155:79–92
- Basu AR, Wang J, Huang W, Xie G, Tatsumoto M (1991) Major element, REE, and Pb, Nd and Sr isotopic geochemistry of Cenozoic volcanic rocks of eastern China: implications for their origin from suboceanic-type mantle reservoirs. *Earth Planet Sci Lett* 105:149–169
- Brenan JM, Neroda E, Lundstrom CC, Shaw HF, Ryerson FJ, Phinney DL (1998) Behaviour of boron, beryllium and lithium during melting and crystallization: constraints from mineral-melt partitioning experiments. *Geochim Cosmochim Acta* 62:2129–2141
- Cabanes N, Mercier JCC (1988) Insight into the upper mantle beneath an active extensional zone: the spinel-peridotite xenoliths from San Quintin (Baja California, Mexico). *Contrib Mineral Petrol* 100:374–382
- Chan LH, Frey FA (2003) Lithium isotope geochemistry of the Hawaiian plume: results from the Hawaii Scientific Drilling Project and Koolau Volcano. *Geochem Geophys Geosyst* 4:337–349
- Chan LH, Edmond JM, Thompson G, Gillis K (1992) Lithium isotopic composition of submarine basalts: implications for the lithium cycle in the oceans. *Earth Planet Sci Lett* 108:151–160
- Chan LH, Alt JC, Teagle DAH (2002) Lithium and lithium isotope profiles through the upper oceanic crust: a study of seawater–basalt exchange at ODP Sites 504B and 896A. *Earth Planet Sci Lett* 201:187–201
- Coltorti M, Bonadiman C, Hinton RW, Siena F, Upton BGJ (1999) Carbonatite metasomatism of the oceanic upper mantle: evidence from clinopyroxenes and glasses in ultramafic xenoliths of Grande Comore, Indian Ocean. *J Petrol* 40:133–165
- Coogan LA, Kasemann SA, Chakrabarty S (2005) Rates of hydrothermal cooling of new oceanic upper crust derived from lithium-geospeedometry. *Earth Planet Sci Lett* 240:415–424
- Dohmen R, Kasemann SA, Coogan L, Chakrabarty S (2010) Diffusion of Li in olivine. Part I: experimental observations and a multi species diffusion model. *Geochim Cosmochim Acta* 74:274–292
- Egging SM, Rudnick RL, McDonough WF (1998) The composition of peridotites and their minerals: a laser-ablation ICP-MS study. *Earth Planet Sci Lett* 154:53–71
- Elliott T, Jeffcoate A, Bouman C (2004) The terrestrial Li isotope cycle: light-weight constraints on mantle convection. *Earth Planet Sci Lett* 220:231–245
- Elliott T, Thomas A, Jeffcoate A, Niu Y (2006) Lithium isotope evidence for subduction-enriched mantle in the source of mid-ocean-ridge basalts. *Nature* 443:565–568
- Fan Q, Hooper PR (1989) The mineral chemistry of ultramafic xenoliths of eastern China: implications for upper mantle composition and the paleogeotherms. *J Petrol* 30:1117–1158
- Frey FA, Green DH (1974) The mineralogy, geochemistry and origin of Iherzolite inclusions in Victorian basanites. *Geochim Cosmochim Acta* 38:1023–1059
- Frey FA, Prinz M (1978) Ultramafic inclusions from San Carlos, Arizona: petrologic and geochemical data bearing on their petrogenesis. *Earth Planet Sci Lett* 38:129–176
- Gallagher K, Elliott T (2009) Fractionation of lithium isotopes in magmatic systems as a natural consequence of cooling. *Earth Planet Sci Lett* 278:286–296
- Gao Y, Casey JF (2012) Lithium isotope composition of ultramafic geological reference materials JP-1 and DTS-2. *Geostandards Geoanal Res* 36:75–81
- Gao Y, Snow JE (2011) Cooling-induced fractionation of mantle Li isotopes from the ultraslow-spreading Gakkel Ridge. *Earth Planet Sci Lett* 301:231–240
- Halama R, John T, Herms P, Hauff F, Schenk V (2011) A stable (Li, O) and radiogenic (Sr, Nd) isotope perspective on metasomatic processes in a subducting slab. *Chem Geol* 281:151–166
- Ionov DA, Seitz HM (2008) Lithium abundances and isotopic compositions in mantle xenoliths from subduction and intra-plate settings: mantle sources vs. eruption histories. *Earth Planet Sci Lett* 266:316–331
- Ionov DA, O'Reilly SY, Genshaft YS, Kopylova MG (1996) Carbonate-bearing mantle peridotite xenoliths from Spitsbergen: phase relationships, mineral compositions and trace-element residence. *Contrib Mineral Petrol* 125:375–392
- Jaques AL, Green DH (1980) Anhydrous melting of peridotite at 0–15 Kb pressure and the genesis of tholeiitic basalts. *Contrib Mineral Petrol* 73:287–310
- Jeffcoate AB, Elliott T, Kasemann SA, Ionov D, Cooper K, Brooker R (2007) Li isotope fractionation in peridotites and mafic melts. *Geochim Cosmochim Acta* 71:202–218
- Johnson KTM, Dick HJB, Shimizu N (1990) Melting in the oceanic upper mantle: an ion microprobe study of diopsides in abyssal peridotites. *J Geophys Res Solid Earth* 95:2661–2678
- Krienitz MS, Garbe Schönenberg CD, Romer RL, Meixner A, Haase KM, Stroncik NA (2012) Lithium isotope variations in ocean island basalts—implications for the development of mantle heterogeneity. *J Petrol* 53:2333–2347
- Lai YJ, Strandmann P, Dohmen R, Takazawa E, Elliott T (2015) The influence of melt infiltration on the Li and Mg isotopic composition of the Horoman Peridotite Massif. *Geochim Cosmochim Acta* 164:318–332
- Lin J, Liu Y, Hu Z, Yang L, Chen K, Chen H, Zong K, Gao S (2016) Accurate determination of lithium isotope ratios by MC-ICP-MS without strict matrix-matching by using a novel washing method. *J Anal At Spectrom* 31:390–397
- Liu JQ (1999) Chinese Volcanoes. Science Press, Beijing (in Chinese)
- Liu DY, Nutman AP, Compston W, Wu JS, Shen QH (1992) Remnants of ≥ 3800 Ma crust in the Chinese part of the Sino-Korean craton. *Geology* 20:339
- Liu YJ, Li MW, Feng ZQ, Wen QB, Neubauer F, Liang CY (2016) A review of the Paleozoic tectonics in the eastern part of Central Asian Orogenic Belt. *Gondwana Res* 43:123–148
- Lundstrom CC, Chaussidon M, Hsui AT, Kelemen P, Zimmerman M (2005) Observations of Li isotopic variations in the Trinity Ophiolite: evidence for isotopic fractionation by diffusion during mantle melting. *Geochim Cosmochim Acta* 69:735–751
- Ma LF, Qiao XF, Min LR, Fan BX, Ding XZ (eds) (2002) *Geology Maps of China*, vol 348. Geology Press, Beijing (in Chinese)
- Magna T, Wiechert U, Grove TL, Halliday AN (2006) Lithium isotope fractionation in the southern Cascadia subduction zone. *Earth Planet Sci Lett* 250:428–443
- Magna T, Ionov DA, Oberli F, Wiechert U (2008) Links between mantle metasomatism and lithium isotopes: evidence from glass-bearing and cryptically metasomatized xenoliths from Mongolia. *Earth Planet Sci Lett* 276:214–222
- Marschall HR, Pogge von Strandmann PAE, Seitz HM, Elliott T, Niu YL (2007) The lithium isotopic composition of orogenic eclogites and deep subducted slabs. *Earth Planet Sci Lett* 262:563–580

- Marschall HR, Wanless VD, Shimizu N, Strandmann P, Elliott T, Monteleone BD (2017) The boron and lithium isotopic composition of mid-ocean ridge basalts and the mantle. *Geochim Cosmochim Acta* 207:102–138
- McDonough WF, Sun SS (1995) The composition of the Earth. *Chem Geol* 120:223–253
- Navon O, Stolper E (1987) Geochemical consequence of melt percolation: the upper mantle as a chromatographic column. *J Petrol* 95:285–307
- Neumann ER, Wulff-pedersen E (1997) The origin of highly silicic glass in mantle xenoliths from the Canary islands. *J Petrol* 38:1513–1539
- Nishio Y, Nakai SI, Yamamoto J, Sumino H, Matsumoto T, Prikhod'ko VS, Arai S (2004) Lithium isotopic systematics of the mantle-derived ultramafic xenoliths: implications for EM1 origin. *Earth Planet Sci Lett* 217:245–261
- Niu YL (1997) Mantle melting and melt extraction processes beneath ocean ridges: evidence from abyssal peridotites. *J Petrol* 38:1047–1074
- Norman MD (1998) Melting and metasomatism in the continental lithosphere: laser ablation ICP-MS analysis of minerals in spinel lherzolites from eastern Australia. *Contrib Mineral Petrol* 130:240–255
- O'Reilly SY, Griffin WL (1988) Mantle metasomatism beneath western Victoria, Australia: I. Metasomatic processes in Cr-diopside lherzolites. *Geochim Cosmochim Acta* 52:433–447
- Penniston-Dorland S, Liu XM, Rudnick RL (2017) Lithium isotope geochemistry. *Rev Mineral Geochem* 82:165–217
- Pogge von Strandmann PAE, Elliott T, Marschall HR, Coath C, Lai Y-J, Jeffcoate AB, Ionov DA (2011) Variations of Li and Mg isotope ratios in bulk chondrites and mantle xenoliths. *Geochim Cosmochim Acta* 75:5247–5268
- Qi L, Hu J, Gregoire DC (2000) Determination of trace elements in granites by inductively coupled plasma mass spectrometry. *Talanta* 51:507
- Richter FM, Davis AM, Depaolo DJ, Watson EB (2003) Isotope fractionation by chemical diffusion between molten basalt and rhyolite. *Geochim Cosmochim Acta* 67:3905–3923
- Richter F, Watson B, Chaussidon M, Mendybaev R, Dan R (2014) Lithium isotope fractionation by diffusion in minerals. Part 1: pyroxenes. *Geochim Cosmochim Acta* 126:352–370
- Rudnick RL, Ionov DA (2007) Lithium elemental and isotopic disequilibrium in minerals from peridotite xenoliths from far-east Russia: product of recent melt/fluid–rock reaction. *Earth Planet Sci Lett* 256:278–293
- Ryan JG, Langmuir CH (1987) The systematics of lithium abundances in young volcanic rocks. *Geochim Cosmochim Acta* 51:1727–1741
- Schuessler JA, Schoenberg R, Srsson O (2009) Iron and lithium isotope systematics of the Hekla volcano, Iceland—evidence for Fe isotope fractionation during magma differentiation. *Chem Geol* 258:79–81
- Seitz HM, Woodland AB (2000) The distribution of lithium in peridotitic and pyroxenitic mantle lithologies—an indicator of magmatic and metasomatic processes. *Chem Geol* 166:47–64
- Seitz HM, Brey GP, Lahaye Y, Durali S, Weyer S (2004) Lithium isotopic signatures of peridotite xenoliths and isotopic fractionation at high temperature between olivine and pyroxenes. *Chem Geol* 212:163–177
- Simons KK, Harlow GE, Brueckner HK, Goldstein SL, Sorensen SS, Hemming NG, Langmuir CH (2010) Lithium isotopes in Guatemalan and Franciscan HP-LT rocks: insights into the role of sediment-derived fluids during subduction. *Geochim Cosmochim Acta* 74:3621–3641
- Su BX, Zhang HF, Sakyi PA, Yang YH, Ying JF, Tang YJ, Qin KZ, Xiao Y, Zhao XM, Mao Q, Ma YG (2011) The origin of spongy texture in minerals of mantle xenoliths from the western Qinling central China. *Contrib Mineral Petrol* 161:465–482
- Su BX, Zhang HF, Deloule E, Sakyi PA, Xiao Y, Tang YJ, Hu Y, Ying JF, Liu PP (2012) Extremely high Li and low $\delta^7\text{Li}$ signatures in the lithospheric mantle. *Chem Geol* 292–293:149–157
- Su BX, Zhang HF, Deloule E, Vigier N, Hu Y, Ying JF, Liu PP (2014a) Distinguishing silicate and carbonatite mantle metasomatism by using lithium and its isotopes. *Chem Geol* 381:67–77
- Su BX, Zhang HF, Deloule E, Vigier N, Sakyi PA (2014b) Lithium elemental and isotopic variations in rock-melt interaction. *Chem Erde* 74:705–713
- Su BX, Zhou MF, Robinson PT (2016) Extremely large fractionation of Li isotopes in chromitite-bearing mantle sequence. *Sci Rep* 6:22370
- Su BX, Chen C, Bai Y, Pang KN, Qin KZ, Sakyi PA (2017a) Lithium isotopic composition of Alaskan-type intrusion and its implication. *Lithos* 286–287:363–368
- Su BX, Zhou XH, Sun Y, Ying JF, Sakyi PA (2017b) Carbonatite-metasomatism signatures hidden in silicate-metasomatized mantle xenoliths from NE China. *Geo J* 53:682–691
- Sun SS, McDonough WF (1989) Chemical and isotopic systematics of oceanic basalts: implications for mantle composition and processes. *Geol Soc Lond Spec Publ* 42:313–345
- Sun H, Gao Y, Xiao Y, Gu HO, Casey JF (2016) Lithium isotope fractionation during incongruent melting: constraints from post-collisional leucogranite and residual enclaves from Bengbu Uplift, China. *Chem Geol* 439:71–82
- Tang YJ, Zhang HF, Ying JF (2007a) Review of the lithium isotope system as a geochemical tracer. *Int Geol Rev* 49:374–388
- Tang YJ, Zhang HF, Nakamura E, Moriguti T, Kobayashi K, Ying JF (2007b) Lithium isotopic systematics of peridotite xenoliths from Hannuoba, North China Craton: implications for melt–rock interaction in the considerably thinned lithospheric mantle. *Geochim Cosmochim Acta* 71:4327–4341
- Tang YJ, Zhang HF, Ying JF (2010) A brief review of isotopically light Li—a feature of the enriched mantle? *Int Geol Rev* 52:964–976
- Tang YJ, Zhang HF, Nakamura E, Ying JF (2011) Multistage melt–fluid-peridotite interactions in the refertilized lithospheric mantle beneath the North China Craton: constraints from the Li–Sr–Nd isotopic disequilibrium between minerals of peridotite xenoliths. *Contrib Mineral Petrol* 161:845–861
- Tang YJ, Zhang HF, Deloule E, Su BX, Ying JF, Xiao Y, Hu Y (2012) Slab-derived lithium isotopic signatures in mantle xenoliths from northeastern North China Craton. *Lithos* 149:79–90
- Tang YJ, Zhang HF, Deloule E, Su BX, Ying JF, Santosh M, Xiao Y (2014) Abnormal lithium isotope composition from the ancient lithospheric mantle beneath the North China Craton. *Sci Rep* 4:4274
- Tatsumoto M, Basu AR, Huang W, Wang J, Xie G (1992) Sr, Nd, and Pb isotopes of ultramafic xenoliths in volcanic rocks of Eastern China: enriched components EMI and EMII in subcontinental lithosphere. *Earth Planet Sci Lett* 113:107–128
- Teng FZ, McDonough WF, Rudnick RL, Walker RJ (2006) Diffusion-driven extreme lithium isotopic fractionation in country rocks of the Tim Mountain pegmatite. *Earth Planet Sci Lett* 243:701–710
- Teng FZ, McDonough WF, Rudnick RL, Wing BA (2007) Limited lithium isotopic fractionation during progressive metamorphic dehydration in metapelites: a case study from the Onawa contact aureole, Maine. *Chem Geol* 239:1–12
- Tomascak PB (2004) Developments in the understanding and application of lithium isotopes in the earth and planetary sciences. *Rev Mineral Geochem* 55:153–195

- Tomascak PB, Tera F, Helz RT, Walker RJ (1999) The absence of lithium isotope fractionation during basalt differentiation: new measurements by multicollector sector ICP-MS. *Geochim Cosmochim Acta* 63:907–910
- Tomascak PB, Widom E, Benton LD, Goldstein SL, Ryan JG (2002) The control of lithium budgets in island arcs. *Earth Planet Sci Lett* 196:227–238
- Tomascak PB, Langmuir CH, Roux PJL, Shirey SB (2008) Lithium isotopes in global mid-ocean ridge basalts. *Geochim Cosmochim Acta* 72:1626–1637
- Tomascak PB, Magna T, Dohmen R (2016) Advances in lithium isotope geochemistry. In: Hoefs J (ed) Advances in isotope geochemistry. <http://dx.doi.org/10.1007/978-3-319-01430-2>
- Vlastélic I, Staudacher T, Bachélery P, Télouk P, Neuville D, Benbakkar M (2011) Lithium isotope fractionation during magma degassing: constraints from silicic differentiates and natural gas condensates from Piton de la Fournaise volcano (Réunion Island). *Chem Geol* 284:26–34
- Webster JD, Holloway JR, Hervig RL (1989) Partitioning of lithophile trace-elements between H_2O and $H_2O + CO_2$ fluids and topaz rhyolite melt. *Econ Geol* 84:116–134
- Wittig N, Baker JA, Downes H (2007) U–Th–Pb and Lu–Hf isotopic constraints on the evolution of sub-continental lithospheric mantle, French Massif Central. *Geochim Cosmochim Acta* 71:1290–1311
- Wunder B, Meixner A, Romer RL, Heinrich W (2006) Temperature-dependent isotopic fractionation of lithium between clinopyroxene and high-pressure hydrous fluids. *Contrib Mineral Petro* 151:112–120
- Xiao Y, Zhang HF, Deloule E, Su BX, Tang YJ, Sakyi PA, Hu Y, Ying JF (2015) Large lithium isotopic variations in minerals from peridotite xenoliths from the eastern North China craton. *J Geol* 123:79–94
- Xiao Y, Zhang HF, Su BX, Zhu B, Chen BB, Chen C, Sakyi PA (2017) Partial melting control of lithium concentrations and isotopes in the Cenozoic lithospheric mantle Jiande area, the Cathaysia block of SE China. *Chem Geol* 466:750–761
- Xu YG, Menzies MA, Vroon P, Mercier JC, Lin C (1998) Texture–temperature–geochemistry relationships in the upper mantle as revealed from spinel peridotite xenoliths from Wangqing, NE China. *J Petrol* 39:469–493
- Xu YG, Menzies MA, Thirlwall MF, Huang XL, Liu Y, Chen XM (2003) “Reactive” harzburgites from Huinan, NE China: products of the lithosphere–asthenosphere interaction during lithospheric thinning? *Geochim Cosmochim Acta* 67:487–505
- Xu R, Liu Y, Tong X, Hu Z, Zong K, Gao S (2013a) In-situ trace elements and Li and Sr isotopes in peridotite xenoliths from Kuandian, North China Craton: insights into Pacific slab subduction-related mantle modification. *Chem Geol* 354:107–123
- Xu WL, Pei FP, Wang F, Meng E, Ji WQ, Yang DB, Wang W (2013b) Spatial–temporal relationships of Mesozoic Volcanic Rock in NE China: constraints on tectonic overprinting and transformations between multiple tectonic regimes. *J Asian Earth Sci* 74:167–193
- Yaxley GM, Crawford AJ, Green DH (1991) Evidence for carbonatite metasomatism in spinel peridotite xenoliths from western Victoria, Australia. *Earth Planet Sci Lett* 107:305–317
- Yu SY, Xu YG, Huang XL, Ma JL, Ge WC, Zhang HH, Qin XF (2009) Hf–Nd isotopic decoupling in continental mantle lithosphere beneath Northeast China: effects of pervasive mantle metasomatism. *J Asian Earth Sci* 35:554–570
- Yu SY, Xu YG, Ma JL, Zheng YF, Kuang YS, Hong LB, Ge WC, Tong LX (2010) Remnants of oceanic lower crust in the subcontinental lithospheric mantle: trace element and Sr–Nd–O isotope evidence from aluminous garnet pyroxenite xenoliths from Jiaohe, Northeast China. *Earth Planet Sci Lett* 297:413–422
- Zack T, Tomascak PB, Rudnick RL, Dalpé C, McDonough WF (2003) Extremely light Li in orogenic eclogites: the role of isotope fractionation during dehydration in subducted oceanic crust. *Earth Planet Sci Lett* 208:279–290
- Zhang M, Suddaby P, O'Reilly SY, Norman M, Qiu J (2000) Nature of the lithospheric mantle beneath the eastern part of the Central Asian fold belt: mantle xenolith evidence. *Tectonophysics* 328:131–156
- Zhang HF, Deloule E, Tang YJ, Ying JF (2010) Melt/rock interaction in remains of refertilized Archean lithospheric mantle in Jiaodong Peninsula, North China Craton: Li isotopic evidence. *Contrib Mineral Petro* 160:261–277